14. Key Words	Link A Role	Link A Wt	Link B Role	Link B Wt	Link C Role	Link C Wt
Thin films						
Semiconductors						
Germanium						
Optical properties						
Epitaxial films						
Optical constants						

ABSTRACT, Continued

A review is given of previous investigations and measurements of the optical properties and constants of germanium thin films. This review shows that the results are much at variance among themselves, due to lack of crystalline perfection in the samples studied. The results for n and k reported in this work were computed from measurements of R and T on a 250A epitaxial germanium film on CaF_2. They are shown to give much better agreement with optical constants from dispersion analysis than those of earlier workers. In addition, with the inclusion of experimental error, the present results overlap those of the dispersion analysis in those wavelength ranges in which it was possible to obtain roots.

Thus, the conclusion of this research may be summarized as follows:

(1) The optical properties of epitaxial germanium films replicate bulk single crystals to a degree sufficient to justify their consideration as vehicles for further optical research into the high energy, high absorption spectral regions.

(2) The use of epitaxial semiconductor films to calculate optical constants will supplement, but not supplant, other methods such as polarimetry and dispersion analysis. (Author)

I have also enjoyed a stimulating and beneficial correspondence concerning various aspects of this research with Billy W. Sloope of the Virginia Institute for Scientific Research and T. M. Donovan of the China Lake Laboratories.

If a student comes into contact with one or two very fine teachers during his years of formal schooling, he is to be considered quite fortunate. It has been my good luck to have had several. Some who influenced my career at an early stage are members of the faculty of Clarkson College of Technology. However, in this instance I refer to Professor William Paul who has been my thesis advisor at Harvard. I shall always be grateful for his editorial assistance in the preparation of this thesis and for his guidance and advice on the experimental problems that arose during the course of this work. The example he has provided of a highly competent research scientist formed a very valuable part of my educational experience at Harvard.

Chapter Five

BIBLIOGRAPHY

[1] J. B. Scarborough, Numerical Mathematical Analysis (The Johns Hopkins Press, Baltimore, 1950) 2nd ed.

[2] A. L. Loeb and H. H. Denman, J. Soc. Indust. Appl. Math. 3, 1 (1955).

[3] R. B. Schoolar and J. R. Dixon (Accepted for publication in Phys. Rev., received Aug. 3, 1964); R. B. Schoolar, Bull. Am. Phys. Soc., Ser. II, 8 516 (1963); P. R. Wessel, Ibid., 516; P. R. Wessel (to be published).

[4] M. Cardona and D. L. Greenaway, Phys. Rev. 133, A1685 (1964).

[5] C. E. Rossi (to be published).

In Chapter Four, Section B, we gave the results for the effect of deposition parameters on the reflectivity and crystallinity of films on fused quartz. These results show that both reflectivity and crystallinity have a strong dependence on substrate temperature and a weak dependence on deposition rate. The crystallinity and reflectivity structure improves with increasing substrate temperature; however, the magnitude of the reflectivity becomes degraded beyond a certain substrate temperature due to increasing roughness effects. In this same section, we also presented the optical response of three epitaxial germanium films on CaF_2. These results indicate interband transition structure corresponding closely to that observed in bulk material, even in the case of films $\sim$ 25 atoms thick.

The results of Chapter Three relating to conclusion (b) above lead us to believe that similar analyses should be undertaken for the dispersion method, polarimetric methods, and other photometric methods in order to determine the efficacy of each for calculating optical constants. The results for the RT method and the two thickness, two transmission method argue eloquently for the necessity of investigating in detail whatever other methods may be chosen in order that experimental conditions may be arranged for optimum results.

It has become apparent since the inception of this research that interest has begun to grow in the optical properties of epitaxial semiconductor thin films. This has been particularly true recently

and dispersion analyses. We have shown that in the region where roots are obtained, the film optical constants compare favorably with the Kramers Kronig result.

With regard to the statement in (a) concerning experimental difficulties, we feel these to be of four types:

(1) Roughness scattering. In Chapters Two and Four we have seen how the presence of granular structure in the film produces scattering effects which reduce reflectivity and destroy coherence. For germanium it appears to be difficult to obtain epitaxial films that do not possess residual roughness. This is because, as pointed out in Chapter Two, Section D, the deposition conditions for epitaxial films are in opposition to the requirements for smooth films. However, there is evidence that the situation is not so severe in the case of epitaxial lead salt films [5]. Roughness is the most serious problem confronting the calculation of the optical constants. However, if the mean film thickness is much larger than the rms surface roughness, its effect may be ignored in transmission and experimentally compensated in reflection. When thickness and roughness are of the same order, coherence is destroyed and it is for this reason that we were unable to apply the two thickness, two transmission method for germanium. Extensions of this research should concentrate on devising methods of producing smooth films, possibly through techniques other than vacuum deposition.

250Å film of Fig. 4-12. The optical constants calculated for the film are shown in Fig. 5-2, where, in performing the calculation, the reflectivity was corrected for roughness according to the experimental quantities $R_\infty = .95\ R_o$ and $\sigma = 50$Å. The bars indicate the error spread in n and k for an absolute error in R of $\pm$ 2.5% and in a of $\pm$ 10Å and a relative error in T of $\pm$ 10%. We see that the discrepancy between the film values of the optical constants and those of bulk Ge (taken from Fig. 1-3b) can be included, for the most part, within the span of these conservative experimental error estimates. We see also that the region in which no roots appeared, namely, 3000Å to 4100Å, corresponds almost exactly to the region predicted by Fig. 3-14a for a 250Å film as having very high sensitivity to experimental errors in R and T. Reference to Figs. 1-5 will show that the present results are far superior to previous film optical constant work, primarily because of the use of epitaxial films.

of equations (3-19) and (3-6) reveals that the number of possible roots is generally indeterminate. This is also shown by the root-locus diagrams Figs. 3-6 through 3-9. The area of n and k to be searched by the program is 0 to 10 for both constants. The program was almost always run in the automatic mode.

Enough iterations were performed so that by using the results of the most recent iteration, the calculated values R', T' would equal the experimental values R, T to within three significant figures. If this did not occur by the 20th iteration, the program would assume that divergence was taking place and print out a statement to this effect along with the results of the last iteration. When the work for the wavelength under consideration was finished, the data for the succeeding one would be read in. After the data had been exhausted, the FORTRAN monitor system automatically terminated the program. The running time to compute the optical constants for 41 wavelengths (6000Å to 2000Å in 100Å intervals) in the automatic mode was approximately two minutes. The calculations for Chapter Three were effected by separately using the arithmetic subroutine which calculates R', T', and the various derivatives.

and that the roots are given by:

$$n = n_o + \Delta n \tag{5-2a}$$

$$k = k_o + \Delta k \tag{5-2b}$$

where Δn and Δk are the necessary corrections to n_o and k_o.

Applying Taylor's theorem to equations (5-1) yields:

$$R(n, k) - R = R(n_o, k_o) - R + (n - n_o)\left(\frac{\partial R}{\partial n}\right)_o + (k - k_o)\left(\frac{\partial R}{\partial k}\right)_o + O(\Delta n^2, \Delta k^2) = 0 \tag{5-3a}$$

$$T(n, k) - T = T(n_o, k_o) - T + (n - n_o)\left(\frac{\partial T}{\partial n}\right)_o + (k - k_o)\left(\frac{\partial T}{\partial k}\right)_o + O(\Delta n^2, \Delta k^2) = 0 \; . \tag{5-3b}$$

If we further assume Δn and Δk to be small enough to neglect their higher-order terms, then we have immediately:

$$n - n_o = \left((R - R(n_o, k_o))\left(\frac{\partial T}{\partial k}\right)_o - (T - T(n_o, k_o))\left(\frac{\partial R}{\partial k}\right)_o \right) / J \tag{5-4a}$$

$$k - k_o = \left((T - T(n_o, k_o))\left(\frac{\partial R}{\partial n}\right)_o - (R - R(n_o, k_o))\left(\frac{\partial T}{\partial n}\right)_o \right) / J \tag{5-4b}$$

where

$$J = \left(\frac{\partial R}{\partial n}\right)_o \left(\frac{\partial T}{\partial k}\right)_o - \left(\frac{\partial R}{\partial k}\right)_o \left(\frac{\partial T}{\partial n}\right)_o \; . \tag{5-5}$$

The roots may now be found to any desired degree of accuracy by repeated applications of these **formulas with the improved values** of n and k substituted at each step. We see that equation (5-5)

[15] H. Brooks, Advances in Electronics and Electron Physics, ed. by L. Larton (Academic Press, New York, 1956), vol. 7; R. W. Keyes, Solid State Physics, ed. by F. Seitz and D Turnbull (Academic Press, New York, 1960), vol. 11.

[16] H. Philipp, W. Dash, and H. Ehrenreich, Phys. Rev. 127, 762 (1962).

[17] W. Paul, J. Appl. Phys. 32, 2082 (1961); R. Zallen and W. Paul, Phys. Rev. 134, A1682 (1964).

[18] M. Cardona and G. Harbeke, J. Appl Phys. 34, 813 (1963).

It is interesting to note that because the force which effects the stress in the film is actually applied at the film-substrate interface, a bending moment arises which tends to lift the film away. This bending moment increases with film thickness until rupture takes place, thus setting an upper limit on the film thickness for a given substrate temperature. For T_S = 600°C, the critical thickness appears to be around 3000Å to 4000Å as deduced from observations of thick films that rapidly broke up immediately after deposition.

4. Comparison with Other Work.

The most recent works on the optical response of thin germmanium films have been by Donovan and Ashley [3], Tauc, et al. [5], and Cardona and Harbeke [18]. The relationship of our work to that of references 3 and 5 has been discussed above. However, in these two the film transmission was not measured. Cardona and Harbeke have measured the transmission (but not reflectivity) of several rather thick epitaxial films on CaF_2. Although their total results account for the proper structure, only one film was thin enough (500Å) for measurements down to the Σ, X transition (which appeared quite weak) and this film did not display the Λ doublet. Also, the magnitude of their transmissivities is in great disagreement with those calculated from bulk optical constants for

$\delta E^{\Lambda}_{[111]} = (-4.0 \times 10^{-6}$ eV/atm) X and $\delta E^{\Lambda}_{[1\ -11]} = (-5.3 \times 10^{-6}$ ev/atm)X. As there are three times as many $\langle 1\ -11\rangle$ transitions as $\langle 111\rangle$, we will take the over-all shift to be the weighted average of $\delta E^{\Lambda}_{[111]}$ and $\delta E^{\Lambda}_{[1\ -11]}$ or $\delta E^{\Lambda} = (-5.0 \times 10^{-6}$ eV/atm)X. From Fig. 4-15, we have $\delta E^{\Lambda} = 44 \pm 10$ millieV as the observed mean shift of the Λ doublet which implies a value of 8800 ± 2000 atm for the induced biaxial compressive stress, as compared with the previously calculated value of 10300 atm from thermal expansion.

E_1 and E_2 for the Σ, X transition are not known at present. However, an estimate can be made of E_1 from the pressure coefficient for the Σ, X transition in silicon measured by Zallen to be $3 \cdot 10^{-6}$ eV/atm [9]. There is an empirical rule which states that among semiconductors with similar band structures, the pressure coefficients for transitions at identical symmetry points of their Brillouin zones are approximately equal [17]. We therefore take Zallen's result to hold for germanium also. For purposes of calculation, we will assume $E_1^X = E_1^{\Sigma}$ and $E_2^{\Sigma} = 0$. From Fig. 4-15, $\delta E^{X,\Sigma} = 33 \pm 12$ millieV which results in X = 16500 ± 6000 atm compressive biaxial stress. The factor of two difference in the Λ and Σ, X results cannot, at present, be attributed to anything except experimental error. Although the shift of the reflectivity was observed in all of our films, it was carefully measured only in the 1850Å film of Figs. 4-11 and 4-15.

[12], with $\Delta T = -575°C$, equations (4-2) and (4-3) give X = 10,800 atm compression.

Brooks's equation for the shift of an energy band under strain may be written as [15]:

$$\delta E = E_1 \, \mathrm{Tr} \, \underline{\underline{u}} + E_2 \, \hat{\underline{k}} \cdot \left(\underline{\underline{u}} - \frac{1}{3} \underline{\underline{1}} \, \mathrm{Tr} \, \underline{\underline{u}}\right) \cdot \hat{\underline{k}} \, . \tag{4-4}$$

Here E_1 and E_2 are deformation potentials (E_1 is directly related to the hydrostatic pressure coefficient), $\hat{\underline{k}}$ is the unit vector in $\underline{k}$ space to the band edge in question and $\underline{\underline{u}}$ is the strain tensor. In the following discussion, we will take δE, E_1, and E_2 to refer to differences in energy transitions instead of band edges. For purposes of discussion, we note that the stress tensor for hydrostatic pressure is

$$\underline{\underline{\sigma}}_{HSP} = -X \begin{pmatrix} 1 & 0 & 0 \\ 0 & 1 & 0 \\ 0 & 0 & 1 \end{pmatrix} \tag{4-5}$$

for which the generalized Hooke's Law in conjunction with (4-4) gives:

$$\delta E = -3 \, E_1 (s_{11} + 2 \, s_{12}) \, X \tag{4-6}$$

where X is of course the pressure. This relates E_1 to $\partial E / \partial P$.

For applied biaxial stress X in the [1 -1 0] and [-1 -1 2] directions, the stress tensor is:

$$\underline{\underline{\sigma}} = \frac{X}{3} \begin{pmatrix} 2 & -1 & -1 \\ -1 & 2 & -1 \\ -1 & -1 & 2 \end{pmatrix} . \tag{4-7}$$

investigate the effect experimentally because of the roughness-coherence difficulties discussed above; however, we would like to make a few conjectures about what might be expected should suitable samples become available. The problem seems to be divided into two aspects: (1) the perturbative effect of the finite boundary on the bulk energy levels, and (2) the "quantitization" of $\underline{k}$ space in the direction normal to the film surface into intervals of $2\pi/Na$ where N is the number of atoms and a the lattice constant. Of these, the second has the interesting possibility of giving the joint density of states a two-dimensional character and of splitting interband transitions which occur between bands of non-zero slope.

3. Effect of Induced Strains in the Films.

Because of the difference in thermal expansion between the film and the substrate, there will appear an induced strain in the film as it is cooled from its formation temperature. The effect of this strain is clear from Fig. 4-5 where it is apparent that both the Λ peaks and the Σ, X peak are shifted to higher energies in the film. In treating this phenomenon, we will make the following idealizations:

(a) The film and substrate will be assumed to be isotropic, homogeneous, and temperature independent in their thermal expansion properties.

poor optical imaging because of the cleaved surface. For the 250Å film of Figs. 4-12 we may perform a similar analysis by using only the reflectivity in the region below 3500Å where interference is small and extrapolating to infinite wavelength. This procedure leads to σ = 50Å and R_∞ = .95 R_o. In addition, we see from Fig. 4-12b that the roughness is not without its effect on the UV transmittance where T of the film falls below its theoretically predicted value by about 50% at λ = 2000Å.

Figure 4-13 shows the optical response of a film whose thickness was measured by infrared transmission to be 135Å. We see that the experimental values of R and T depart considerably from the corresponding theoretical values for this thickness, T measured being higher than T calculated (except in the far UV region) with the reverse true for R. This behavior was observed in each of our very thin films, thus the film of Fig. 4-13 is not a mere variant. The RED pattern for this film shows sharp Laue spots indicating epitaxy, and Fig. 4-13 confirms the presence of the appropriate interband structure. The disparity in amplitudes is probably due to the breakdown of coherent interference effects when the RMS roughness of the film approaches an appreciable fraction of the mean film thickness. This results in phase averaging or intensity addition (discussed in Chapter Three) for the theoretical R and T expressions. The scattering will not be as strong for IR

well as roughness degrade the reflectivity. However, according to Chapter Two, Section D, amorphous films should be smoothest of all. If this is true, then the reflectivity of amorphous films should be the same as that of smooth bulk crystalline surfaces in the far ultraviolet, as the optical response in this region is due to valence band plasma oscillations which are relatively independent of long-range order. This has been observed to be the case by Tauc, et al. [5], who also explain the deviation of the Σ, X peak amplitude (whose reflectivity was 55%) of their polycrystalline film from the bulk value as due to surface roughness scattering.

Figures 4-8 and 4-9 give the results of the multideposition rate series of films on fused quartz. We see that this parameter does not influence either crystalline quality or reflectivity as strongly as does T_S. All of the RED patterns appear identical except for intensity differences caused by variations in exposure times. The differences in amplitude among the Σ, X peaks may or may not be significant. Their magnitudes and shapes are nearly identical. The most cautious conclusion would seem to be that over the range of Δ shown, the film crystalline and optical properties are reasonably constant.

In Chapter Two, Section D, evidence for the presence of surface roughness for epitaxial films on CaF_2 was given. In Fig. 4-11, we see that the reflectivity of the 1850 Å film, thick enough to

Ashley [3] have studied this problem using polycrystalline films and polished bulk surfaces, and on the basis of their results have suggested that in the bulk material "the observed structure in the reflectance in the region of 2 eV results from a combination of the L and Λ transitions or that the 2.3 eV peak corresponds to transitions at the Λ point and the peak at 2.1 eV corresponds to transitions at the L point." That neither of these deductions is wholly correct can be reasoned as follows:

(a) Neither explanation accounts in a clear manner for the theoretically predicted spin orbit splitting [7].

(b) The calculations of Brust [8] indicate that the $L_3' \rightarrow L_1$ transition has a joint density of states of Type M_o which has the wrong shape to cause a peak in the reflectivity spectrum.

(c) Pressure measurements of Zallen [9] show that both peaks have the same pressure coefficient, as would be expected if they arose at the same point in the band.

(d) The L transitions have actually been observed apart from the Λ transitions by Greenaway [10] for GaAs and by Cardona and Greenaway [11] for ZnTe and CdTe.

In the case where the peaks are distorted due to polycrystalline film structure or polished bulk surfaces, a simpler explanation of either increasing the relative difference between the amplitudes of the two peaks or reversing their magnitudes is

structure indicated by the bulk reflectivity, including the Λ spin-orbit splitting. This is most strikingly brought out by Fig. 4-11 for the 1850 Å film (the shift of the Λ peaks will be discussed later in Subsection 3). Even the 135 Å film, which is only about 25 atoms thick, reveals the structure predicted by bulk measurements, and, in fact, the proper structure was also observed in still thinner epitaxial films. The RED patterns indicate the presence of stacking faults and twins in each of our epitaxial films; however, their effect on the film optical response is not known at the present time.

The RED results for the **multisubstrate temperature series on** fused quartz show a progression from sharp, textured Debye-Scherrer-Hull rings at 780°C to broad, diffuse DSH rings at 25°C, as indicated in Fig. 4-6. At the higher temperatures, one can see regular intensification of the rings which signify the presence of ⟨110⟩ preferred orientation in the film normal to the substrate. Thus,we see that the higher the substrate temperature, the greater the crystalline ordering, in agreement with the discussions of Chapter Two. The reflectivity structure of this series shows a strong temperature dependence. Referring to Fig. 4-7, the 780°C film, curve 1, possesses all of the bulk structure, except that the Λ spin-orbit split peaks are severely distorted. As T_S decreases, clear evidence of these peaks disappears; however, the

and the data recorded. Films having relatively high reflectivity at 2800 Å were scanned to obtain their entire reflectivity spectrum from 2000 Å to 6000 Å, and, if thin enough, their transmissivities were also measured. Figure 4-10 shows the RED patterns and Figs. 4-11, 4-12, and 4-13 the optical response of three typical films differing widely in thickness. These films are by no means to be regarded as unique occurrences; in fact, in each case other films were made under identical conditions and they displayed nearly the same optical response as those shown. Deposition rates and substrate temperatures were kept reasonably constant at values thought to produce films with minimum roughness yet good crystalline quality (see Chapter Two).

Optical measurements were also made on three films received from the University of Virginia Materials Science Department [4]. These films were grown under conditions of substrate temperature 300°C and ambient pressure $5 \cdot 10^{-8}$ torr. When these films were examined by RED, they were epitaxial but contained a superposed twin patterns whose spots were almost as intense as the basic (111) Laue pattern. The usual interband transition structure in the reflectivity spectrum was quite weak and none of the films displayed distinctly the spin-orbit split Λ peaks. None of the films was thin enough for transmission measurements.

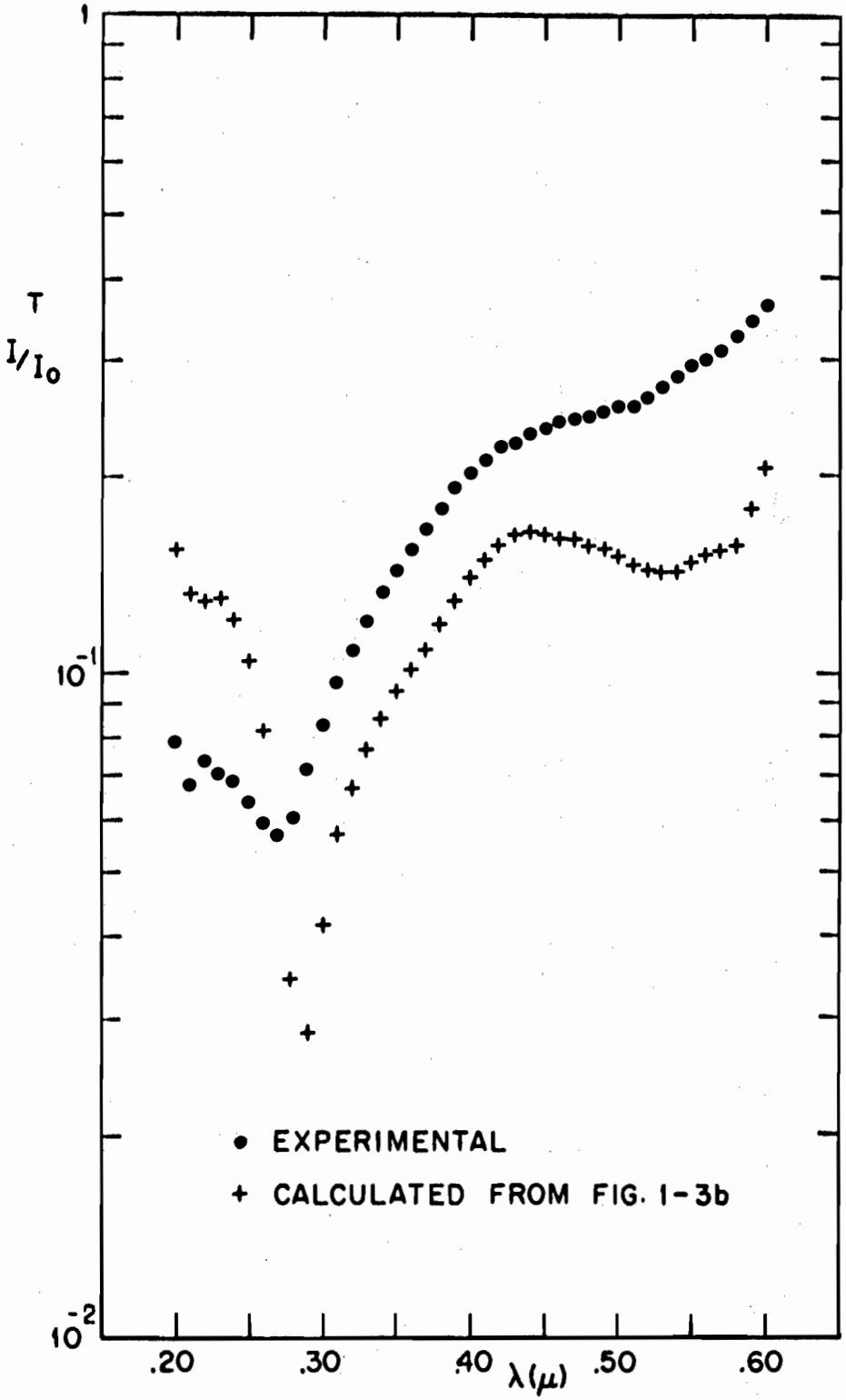

FIG. 4-13b TRANSMISSION OF A 135Å EPITAXIAL GERMANIUM FILM ON CaF_2.

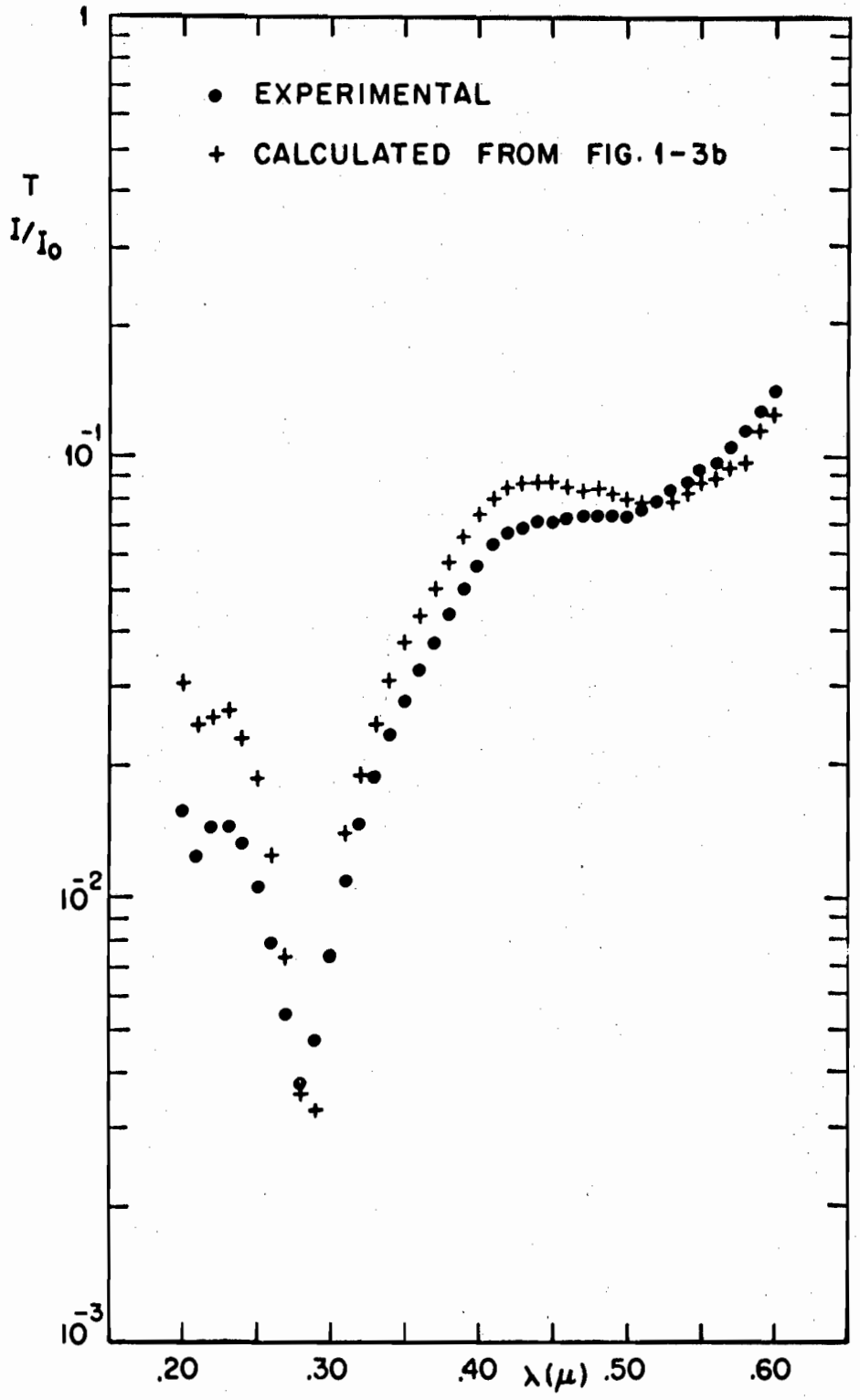

FIG. 4-12b TRANSMISSION OF A 250Å EPITAXIAL GERMANIUM FILM ON CaF2.

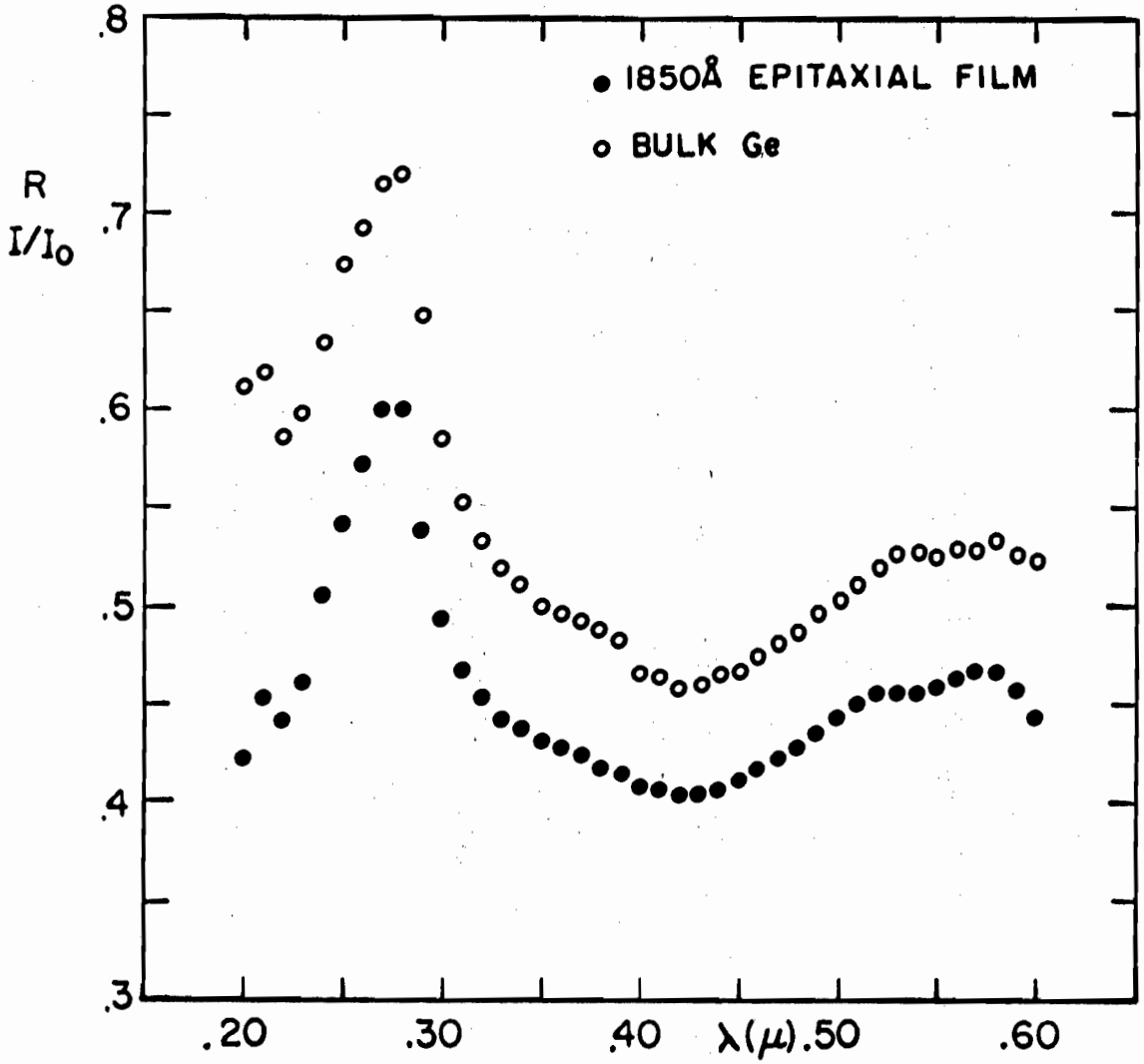

FIG. 4-11 REFLECTIVITY OF A 1850Å EPITAXIAL GERMANIUM FILM COMPARED WITH THAT OF BULK GERMANIUM.

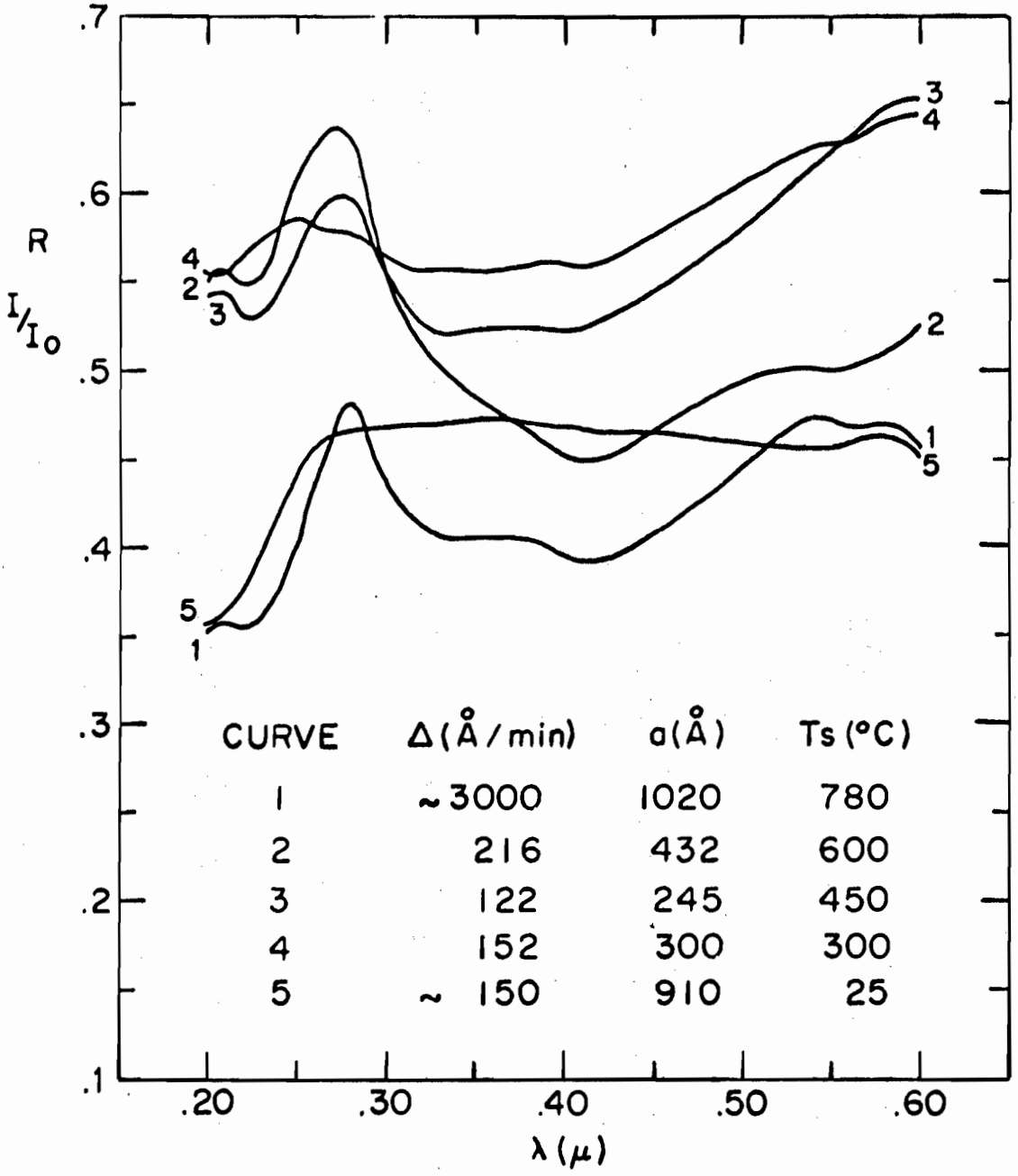

FIG. 4-7 REFLECTIVITY OF Ge FILMS ON FUZED QUARTZ FOR VARIOUS SUBSTRATE TEMPERATURES, Ts.

because the light is converging to a focus on the sample and also because of the irregular substrate surface. The error due to these effects is estimated to be approximately $\pm 10\%$ relative.

B. RESULTS FOR THE REFLECTIVITY AND TRANSMISSIVITY COEFFICIENTS

1. Results for Fused Quartz Substrates.

It was decided to study the reflectivity of germanium films deposited on fused quartz substrates for the following reasons:

(a) To ascertain whether or not such films might possibly make more suitable vehicles for the calculation of the optical constants than those on CaF_2.

(b) To check our experimental methods by comparing our results with a similar, but less complete study by T. M. Donovan and E. J. Ashley [3].

Two sets of experiments were performed, one being the maintenance of a reasonably constant deposition rate, denoted by Δ, while the substrate temperature, denoted by T_S, was varied considerably, and the other being of the same type except that T_S was held constant and Δ varied. Figure 4-6 gives the RED patterns and Fig. 4-7 the reflectivity as T_S was varied, while Figs. 4-8 and 4-9 hold for the case in which Δ was varied. The method of deposition was the same as outlined in Chapter Two, Section B-3. However, the substrate preparation differed in that all substrates

approaches that of reference 1. Our method was to obtain a 1 cm × 1 cm × 1 mm slab of 40 Ω·cm high purity single crystal of germanium with its surface parallel to the {111} planes of the crystal. This slab was then attached to a lapping dop and the following procedure used:

(a) The sample was first lapped with 12 μ Buehler #1200 lapping compound.

(b) Lapping was completed with 3 μ Al_2O_3.

(c) Polishing commenced with .3 μ Linde "A" using a beeswax polishing platform.

(d) Polishing was completed with .1 μ Linde "B", also on beeswax. Great care was taken during this step not to bear undue pressure on the sample and hence to minimize the depth of the amorphous surface layer left by polishing. Each step was continued for such time as was felt necessary to remove the damaged layer incurred by the previous step.

After polishing, the sample was removed from the dop for etching. A fresh batch of CP-4 was prepared, the sample placed in a Teflon dish, and about 15 cc of the solution poured over it. The acid was gently sloshed over the sample for one minute, whereupon the etching was stopped with distilled H_2O. The sample was then cleaned in three changes of fresh acetone and finally swabbed with a benzene soaked Q-tip. The sample was immediately placed in a sample holder, alignment made through use of the above procedure,

These conditions closely approximate those under which transmission measurements on germanium films were made. The scattered light determined in this way was found to be .08%. This effectively limited the dynamic range of the spectrophotometer to about three orders of magnitude.

2. Description of Experimental Procedure. Test and Calibration by Measurement of Bulk Reflectivity.

As was mentioned above, the measurement of absolute reflectivity by our apparatus depends on whether or not the optical paths $S \rightarrow M_T \rightarrow PM$ and $S \rightarrow M_R \rightarrow PM$ are equivalent. Also, from Fig. 2-4 we see that we are seeking the reflectivity of a highly irregular surface caused by the presence of cleavage steps in the substrate. Therefore, the following experimental procedure was used:

(a) With the sample removed, light with wavelength 5300Å was allowed to fall upon mirror M_T. Since the light is focused at S, a short distance from M_T, M_T collects all of the incident light. M_T is now rotated until it floods the photomultiplier cathode with the maximum amount of light as found by optimizing the photomultiplier output.

(b) The sample, mounted in a sample holder as shown in Fig. 4-4, is now placed into position. It is then situated so that the film surface stands halfway between mirrors M_T and M_R. M_R is then rotated in order to optimize the signal output as in (a).

the randomly distributed phase of the input noise causes it to be attenuated to a greater or lesser degree. In our system, the appropriate reference signal is generated by a photodiode-panel light assembly mounted on the chopper wheel housing. The light from the panel light is chopped and then detected by the photodiode. The phase difference between this signal and the chopped light signal from the monochromator exit slits is controlled by mechanically moving the photodiode-panel light assembly along the circumference of the chopper wheel housing. The output of the photodiode is now symmetrized by a transistor switching circuit. It is then fed to a waveform shaping filter whose function is to isolate the fundamental sinusoidal harmonic of the reference signal so that it can be operated on by the phase shifting network which follows the filter. This circuit provides an additional means for adjusting the phase difference between the input signal and the reference signal. The reference signal next triggers a single-shot multivibrator whose purpose is to provide a large amplitude square wave with fast rise and fall times to be used in switching the diodes of the phase sensitive detector. This detector has been so designed that in effect it full-wave rectifies the "intelligence" portion of the input signal and yields an output which is independent of the amplitude of the reference signal. The average value of the phase sensitive detector output is found by passing

used for all optical measurements in the spectral range 6000Å-2000Å was a model 6256B manufactured by EMI, Ltd. of the United Kingdom. This tube has a 1 cm diameter quartz window with an S-13 response cathode. It has a particularly low dark current and very high gain.

Let us now consider Fig. 4-1b which shows the flow paths of the electronic signals from the photomultiplier and the chopper photodiode. Because a photomultiplier is principally a constant current source, the usual practice is to convert the current signal into a voltage signal with the anode resistor R_A. This also provides a means of controlling the system gain. In our system, we used two values of R_A, 1K and 10K, providing a gain or attenuation capability of 10 in the input voltage signal. This signal is fed through the coupling capacitor C_A into a negative feedback amplifier tuned with a twin T filter to a narrow passband around 1080 cps. The open loop gain of this amplifier is high enough so that the closed loop gain is dependent only on the passive elements of the twin T filter. The second stage of amplification is another negative feedback amplifier with RC cutoffs on both the high and low frequency sides of 1080 cps in order to complement the twin T filter of the first stage. The purpose of this extensive filtering is to reduce the amount of noise in the signal eventually to be detected. The "intelligence" in the incoming signal consists

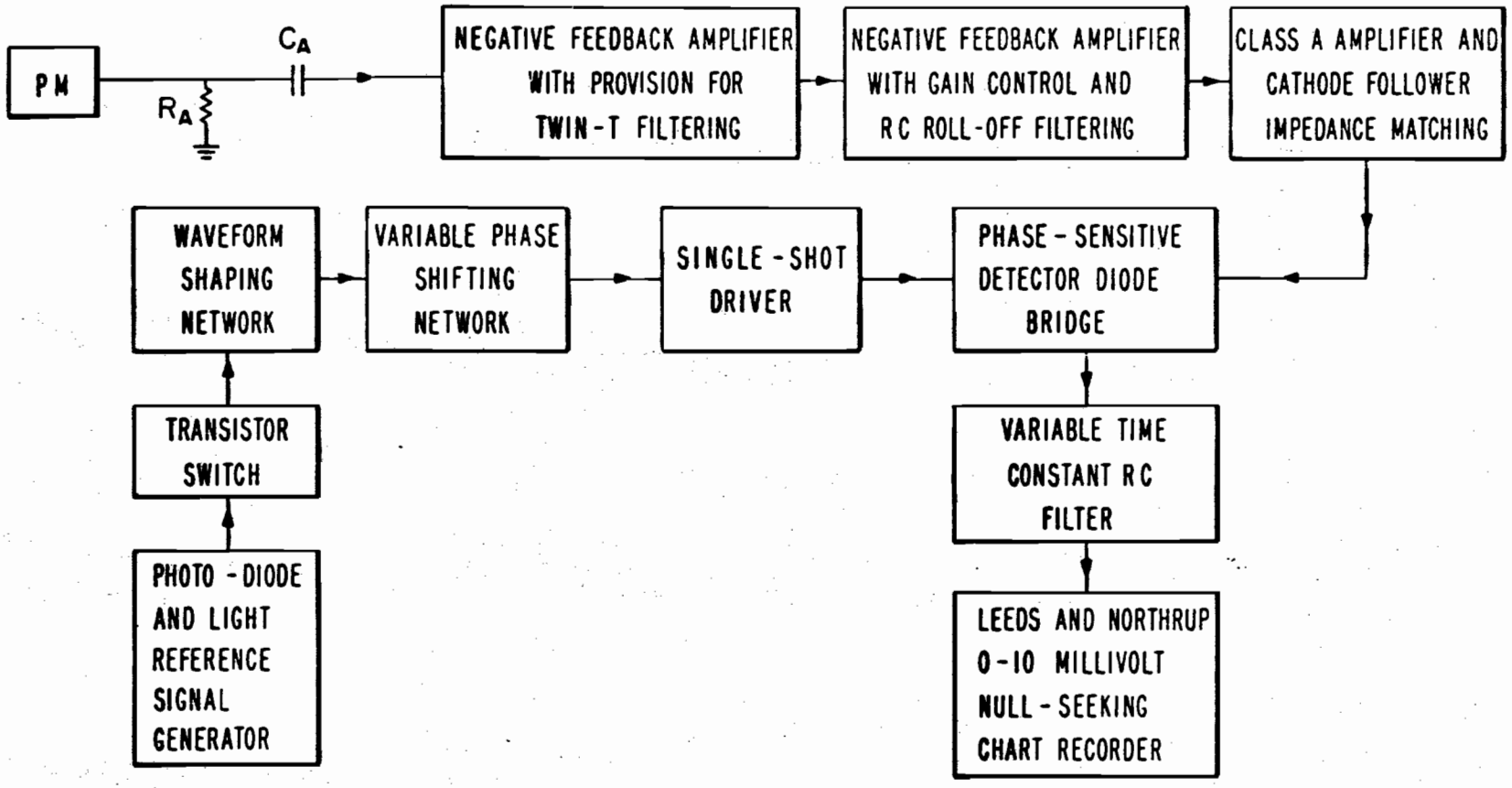

FIG. 4-1b BLOCK DIAGRAM OF THE ELECTRONIC SIGNAL PATH.

Bausch and Lomb grating blazed at 5000Å producing a linear dispersion of 16Å /mm at the exit slit. The lamps used as sources were a General Electric instrument lamp, type 9A/T8½/1, and a high pressure deuterium discharge lamp, model D-100-S, manufactured by Quarzlampen G.m.B.H., Hanau, West Germany. The GE lamp, with a 1 mm × 1 in. tungsten filament, was used for the spectral range 6000 to 3500Å, while the deuterium lamp, with a 1 mm circular aperture, was used for the spectral range 4000Å to 2000Å. For most of the optical experiments, an entrance and exit slit width of 100 μ and a slit height of 5 mm, giving a resolution of 1.6Å, were found to provide sufficient light intensity without overloading the detector and electronics or unduly increasing the scattered light. Also, a scanning rate of 125Å /m in for the entire spectral range covered was found to be a good compromise in that it provided data for the over-all picture fairly rapidly, and was sufficiently slow that any fine structure present would be observed.

Upon emerging from the monochromator exit slit, the light is chopped at a frequency of 1080 cps by a rotating slotted wheel. Attached to the chopper C is a panel light-photodiode combination whose purpose is to provide an electronic signal with a constant phase relationship to the chopped optical beam. The chopper light is now reflected by mirror M_3 to the "mirror lens" system comprised of mirrors M_4, M_5, and M_6. The magnification of the mirror

Chapter Three

BIBLIOGRAPHY

[1] F. Martens, Ann. Physik 6, 606 (1901).

[2] H. R. Philipp, **private communication**, Nov. 16, 1964.

[3] T. M. Donovan, E. J. Ashley, and H. E. Bennett, J. Opt. Soc. Am. 53, 1403 (1963).

[4] J. F. Hall and W. F. C. Ferguson, J. Opt. Soc. Am. 45, 714 (1955).

[5] L. Harris and A. L. Loeb, J. Opt. Soc. Am. 45, 179 (1955).

[6] P. R. Wessel, to be published.

[7] L. Harris, J. K. Beasley, and A. L. Loeb, J. Opt. Soc. Am. 41, 604 (1951).

[8] W. H. Brattain and H. B. Briggs, Phys. Rev. 75, 1705 (1949).

[9] H. A. Gebbie, Ph.D. Thesis (unpublished), Reading, 1952.

[10] H. R. Philipp and H. Ehrenreich, Phys. Rev. 129, 1550 (1963).

[11] M. Cardona and D. L. Greenaway, Phys. Rev. 133, A1685 (1964).

[12] H. Ehrenreich and H. R. Philipp, Phys. Rev. 128, 1622 (1962).

[13] H. Ehrenreich, H. R. Philipp, and B. Segall, Phys. Rev. 132, 1918 (1963).

[14] P. M. Grant, Bull. Am. Phys. Soc. 10, Series II, 546 (1965).

[15] F. Herman, J. Electronics 1, 103 (1955); M. Cardona, Phys. Rev. 129, 69 (1963).

the λ^2 law of the isoelectronic sequence [15].† Also there is evidence that SnTe, GeTe, and the semimetals As, Sb, and Bi may have such an energy [11] in addition to some metals [12, 13].

On the other hand, it appears possible with the two transmission, two thickness method to choose a pair of films that will reduce the error derivatives to a tolerable size for all wavelengths to be considered in this work. Thus it seems that this method is superior to the RT method. However, it was pointed out that our method of presentation would probably favor this technique; therefore, it still remains a matter to be decided by experiment in order to see which of the two techniques is the better.

---

† It is interesting to note that the relation $\epsilon_1 = 1$ has the following connection with the fundamental processes of a material. From the definition $\tilde{\epsilon} = 1 + 4\pi\tilde{\chi}$, we see that if $\epsilon_1 = 1$, $\chi_1 = 0$. Now if we consider an electromagnetic wave with frequency ω incident on a collection of N classical harmonic oscillators with charge-mass ratio e/m, characteristic frequency ω_o, and damping time τ, we have:

$$\chi_1 = Ne^2/m \frac{\omega_o^2 - \omega^2}{(\omega_o^2 - \omega^2)^2 + \frac{\omega^2}{\tau^2}}$$

$$\chi_2 = Ne^2/m \frac{\omega/\tau}{(\omega_o^2 - \omega^2)^2 + \frac{\omega^2}{\tau^2}} \quad .$$

We see that this implies that when $\epsilon_1 = 1$, our incident light frequency is passing through the resonance frequency of the oscillators. We note also that in the region of plasma oscillations, $n \approx k$.

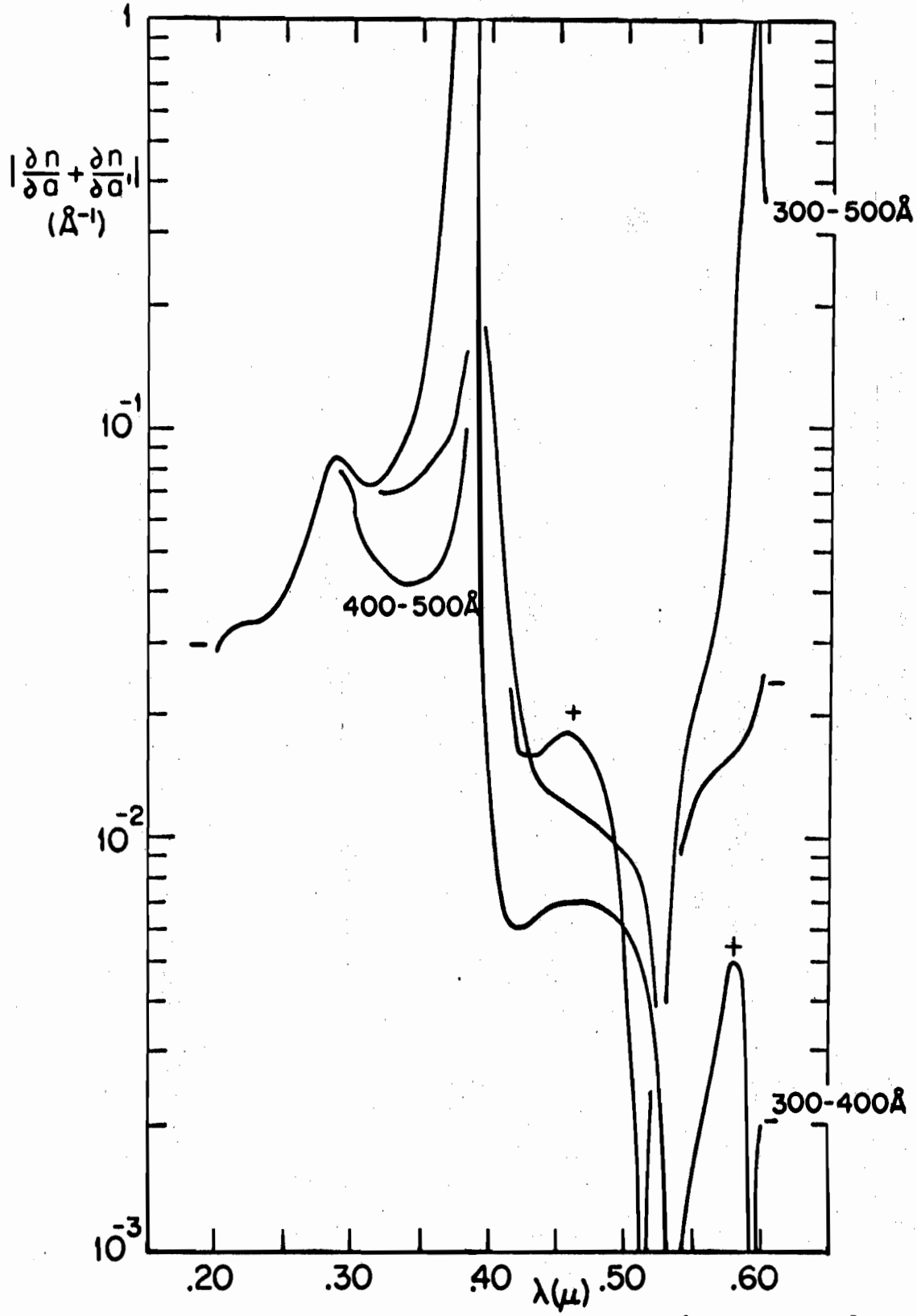

FIG. 3-17d a' PAIRED WITH a = 300Å AND 400Å.

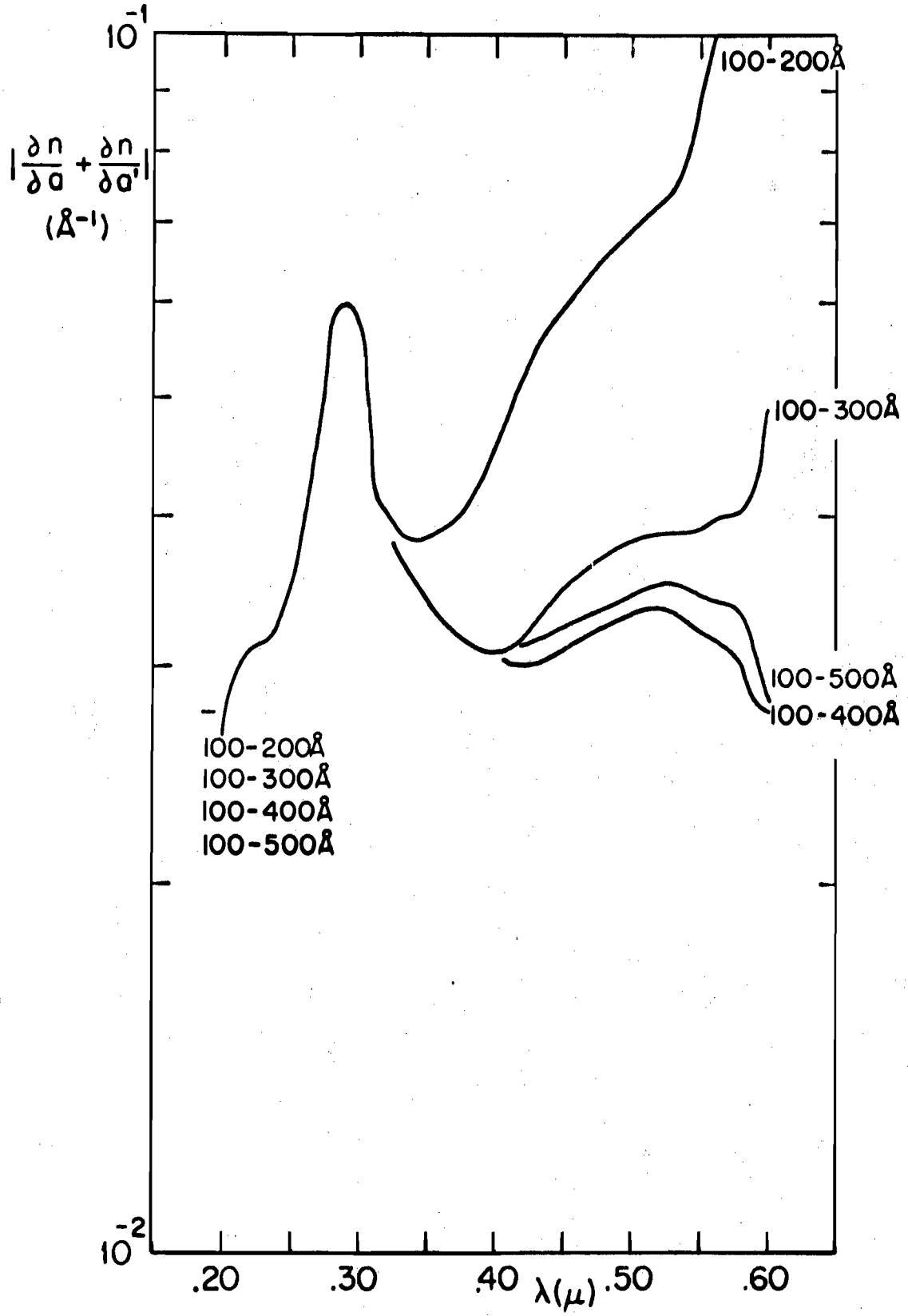

FIG. 3-17b a′ PAIRED WITH a = 100Å.

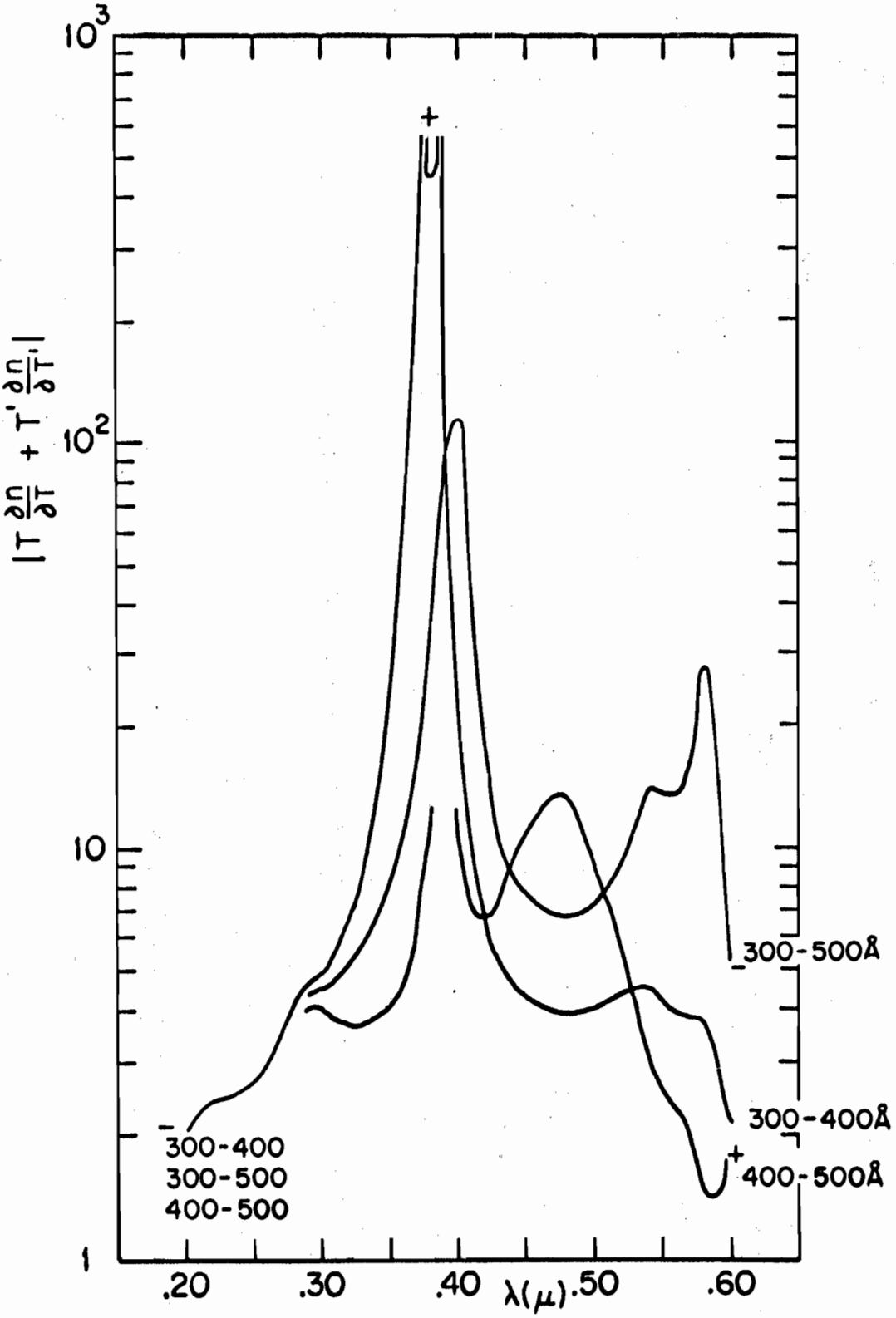

FIG. 3-16d a′ PAIRED WITH a = 300Å AND 400Å.

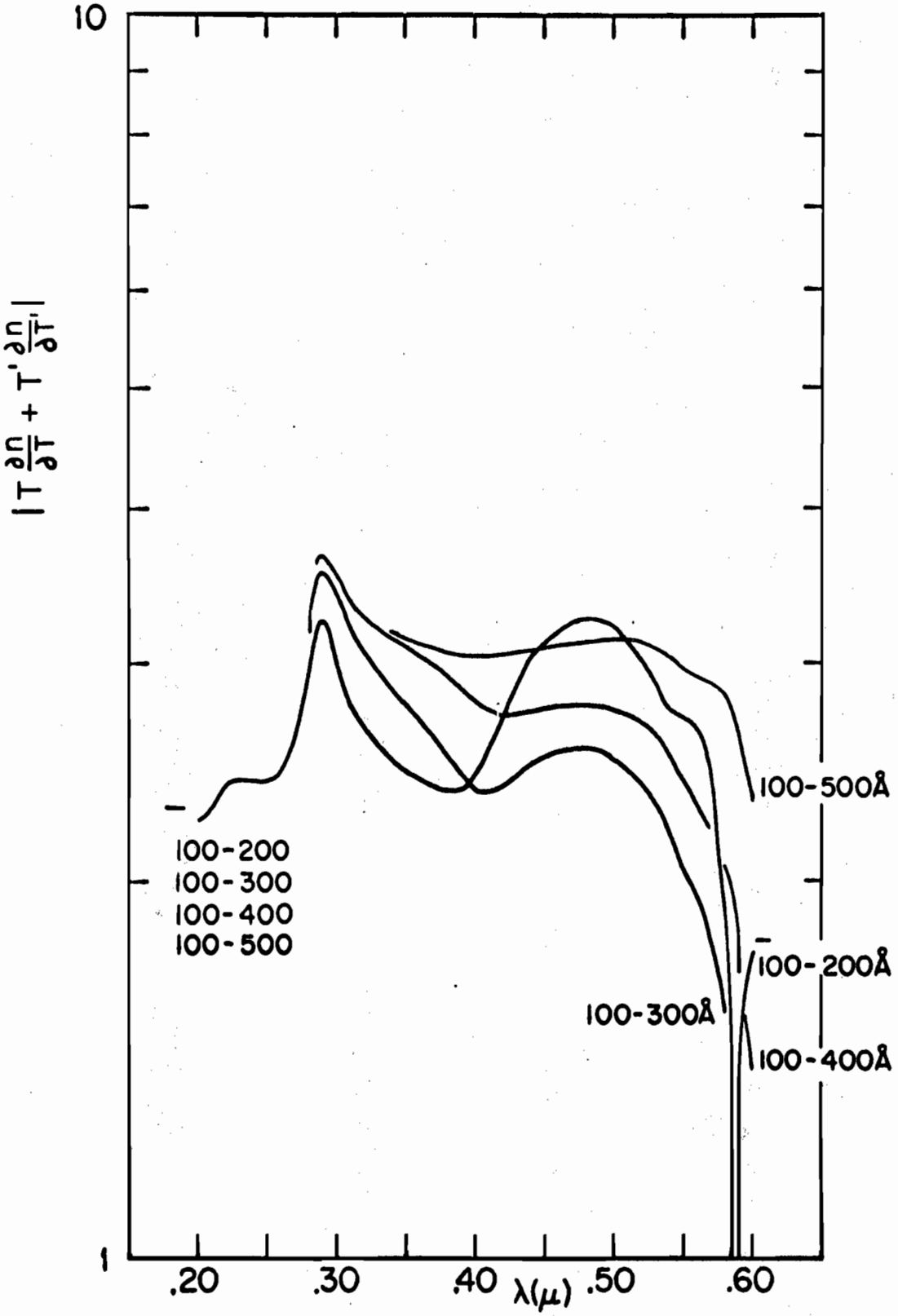

FIG. 3-16b a′ PAIRED WITH a = 100Å.

enough to cause errors greater than $\pm.5$ in the deduced optical constants, but that their sum almost completely cancels any effect. We have also assumed that we can combine the thickness error derivatives into a single quantity $\left| \frac{\partial n}{\partial a} + \frac{\partial n}{\partial a'} \right|$ by considering $da = da'$. The experimental motivation in this case, however, is less clear than in the former, although if we measure the thickness by infrared transmission, the justification becomes the same as above. Again we have the possibility that our means of presentation unduly favors the two thickness, two transmission method because $\left| \frac{\partial n}{\partial a} \right| \approx \left| \frac{\partial n}{\partial a'} \right|$ with their signs opposing. Figures 3-16 and 3-17 show the behavior of the combined error derivatives with wavelength. They are plotted as a family of curves for **representative thickness pairs.** Note that, although there are no **singularities in the region near** $n^2 = k^2 + 1$, almost every curve has at least a relative maximum in this area.

We see that there exists the possibility of choosing an optimum thickness pair with which the effect of experimental errors on the deduced optical constants will be minimized. In fact, for $a = 100\text{Å}$, $a' = 300\text{Å}$ or 400Å, the combined error derivatives have values below the limits imposed by the considerations of Section A-2. Therefore, it appears that measurements on pairs of films with the above thicknesses would yield reasonably accurate values of the optical constants.

thicknesses. This was the approach used by Brattain and Briggs [8] and Gebbie [9] to obtain the optical constants of germanium films. In reality the method requires four measurements altogether as one must also determine the thicknesses of the two films involved. The appropriate equations are:

$$T = T(n, k; \lambda; a) \tag{3-22a}$$

$$T' = T(n, k; \lambda; a') \tag{3-22b}$$

where the functional dependence of the right-hand side is given by equations (3-4) and (3-6b). The left-hand side represents the experimental or measured quantities.

2. Error Derivatives

Following the method of Section A-2 we may write the appropriate differentials as:

$$dn = \frac{\partial n}{\partial T} dT + \frac{\partial n}{\partial T'} dT' + \frac{\partial n}{\partial a} da + \frac{\partial n}{\partial a'} da' \tag{3-23a}$$

$$dk = \frac{\partial k}{\partial T} dT + \frac{\partial k}{\partial T'} dT' + \frac{\partial k}{\partial a} da + \frac{\partial k}{\partial a'} da' \ . \tag{3-23b}$$

Almost the entire discussion of Section A-2 as it applies to the method of finding the error derivatives is valid here. Also, the root-locus approach as given in Section A-2 may be brought over to this method if so desired. Furthermore, we could consider the two thickness, two transmission technique with the aid of the simpler film models; however, such an attack does not seem to yield any

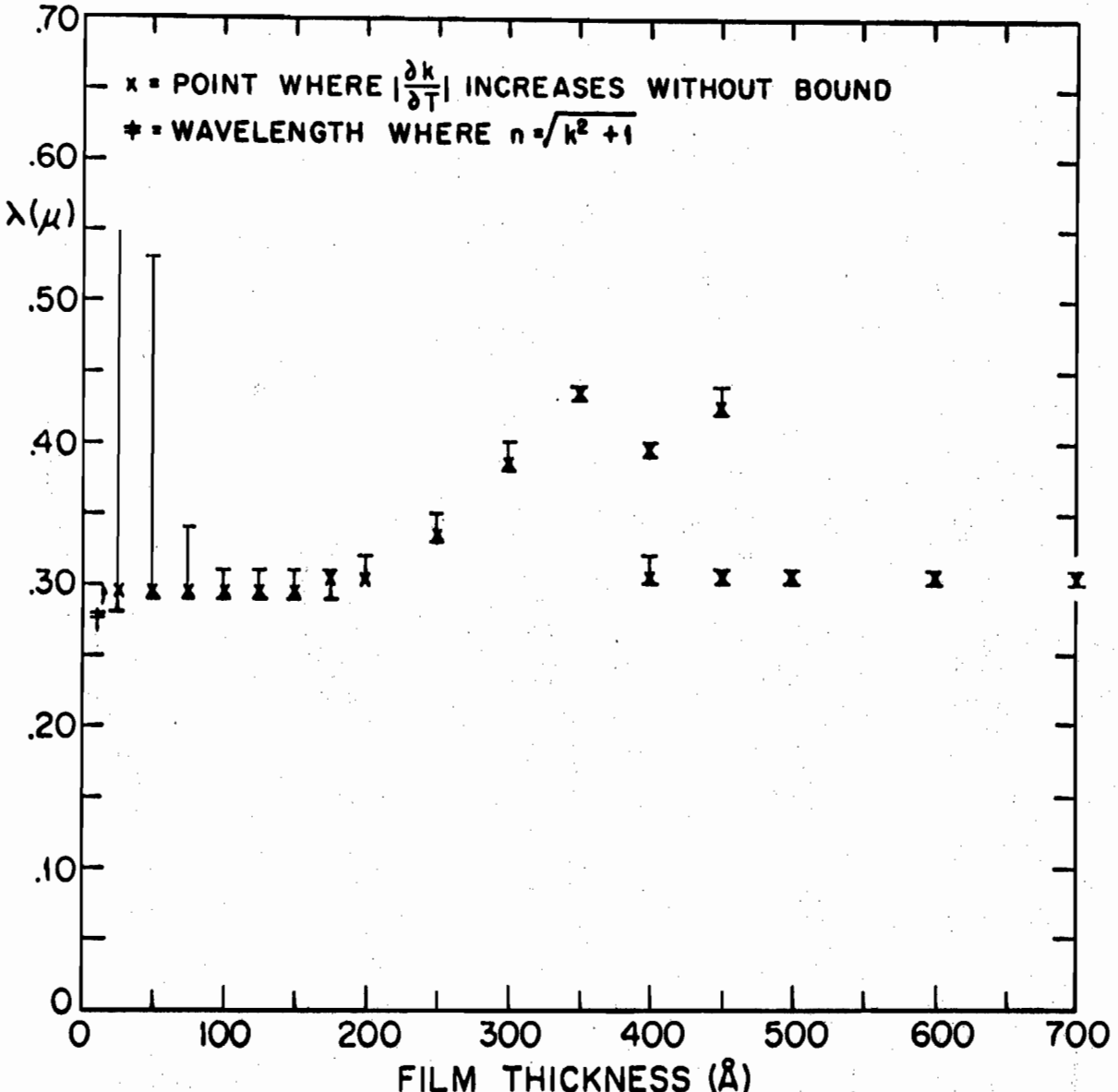

FIG. 3-15b WAVELENGTH REGION WHERE $T|\frac{\partial k}{\partial T}| \geq 5$ FOR THE R-T MODEL OF A Ge FILM ON CoF_2.

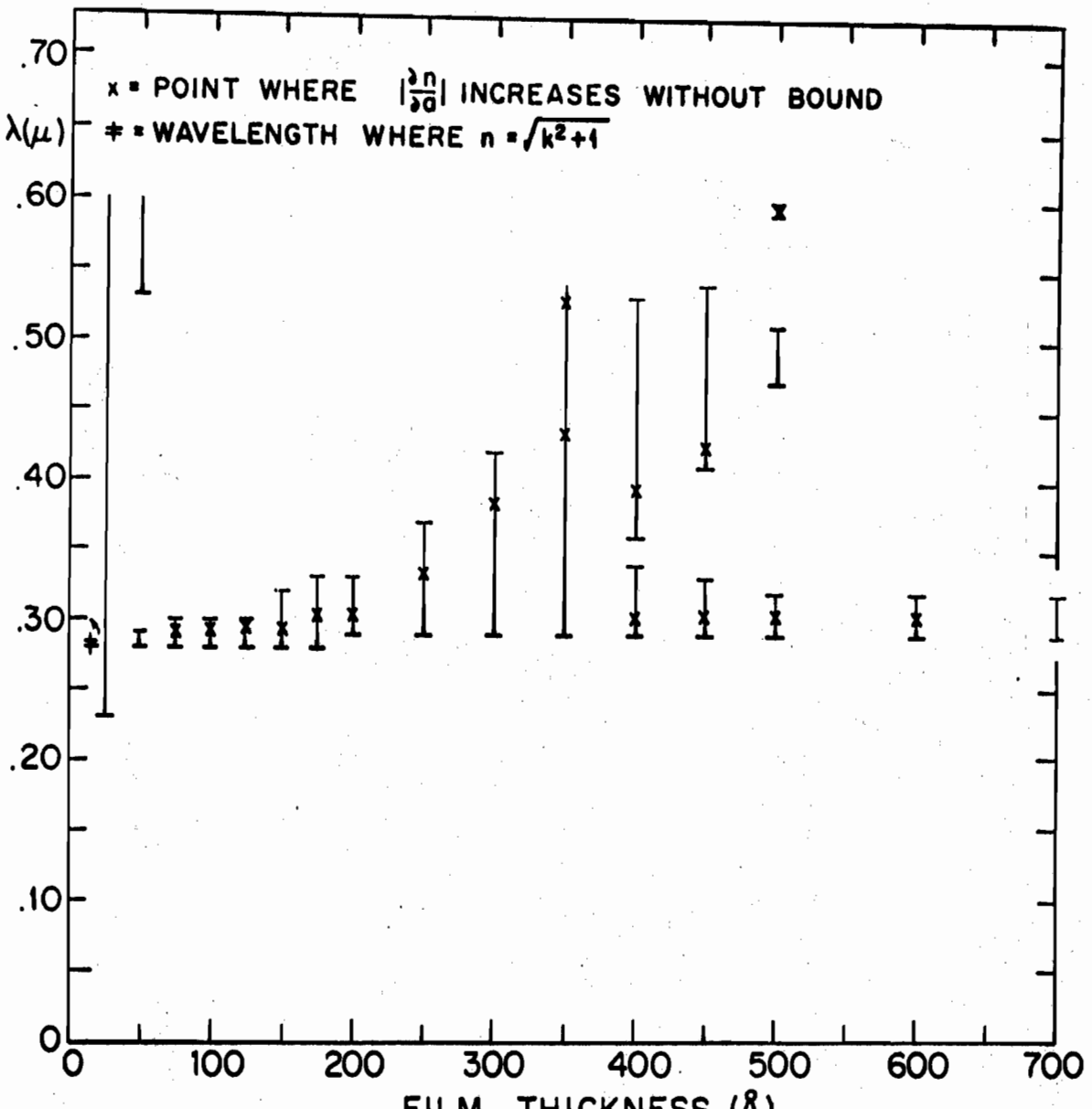

FIG. 3-14c WAVELENGTH REGION WHERE $|\frac{\partial n}{\partial a}| > 5 \cdot 10^{-2}/\text{Å}$ FOR THE R-T MODEL OF A Ge FILM ON CaF_2.

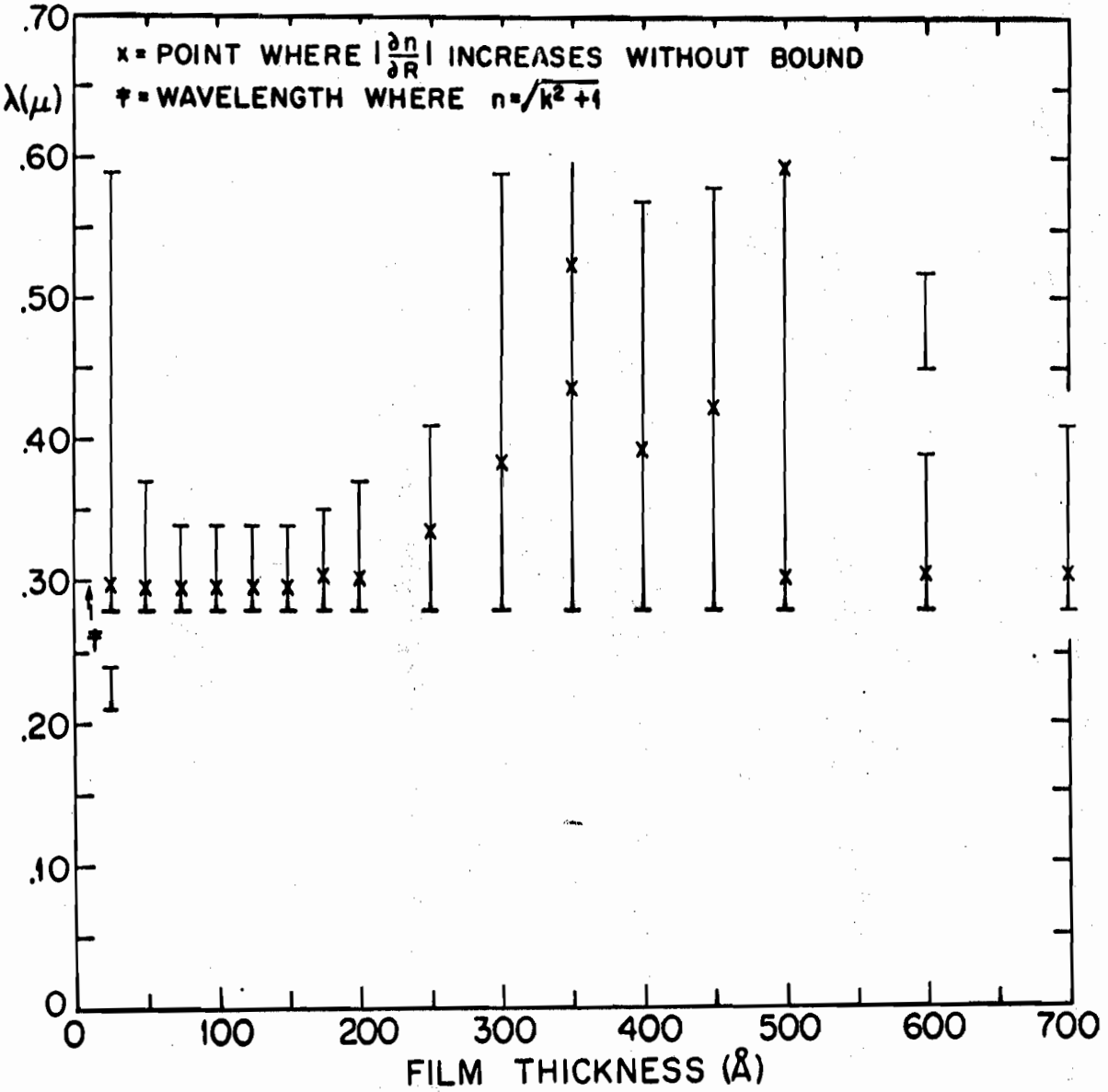

FIG. 3-14a WAVELENGTH REGION WHERE $|\frac{\partial n}{\partial R}| \geq 20$ FOR THE R-T MODEL OF A Ge FILM ON CaF_2.

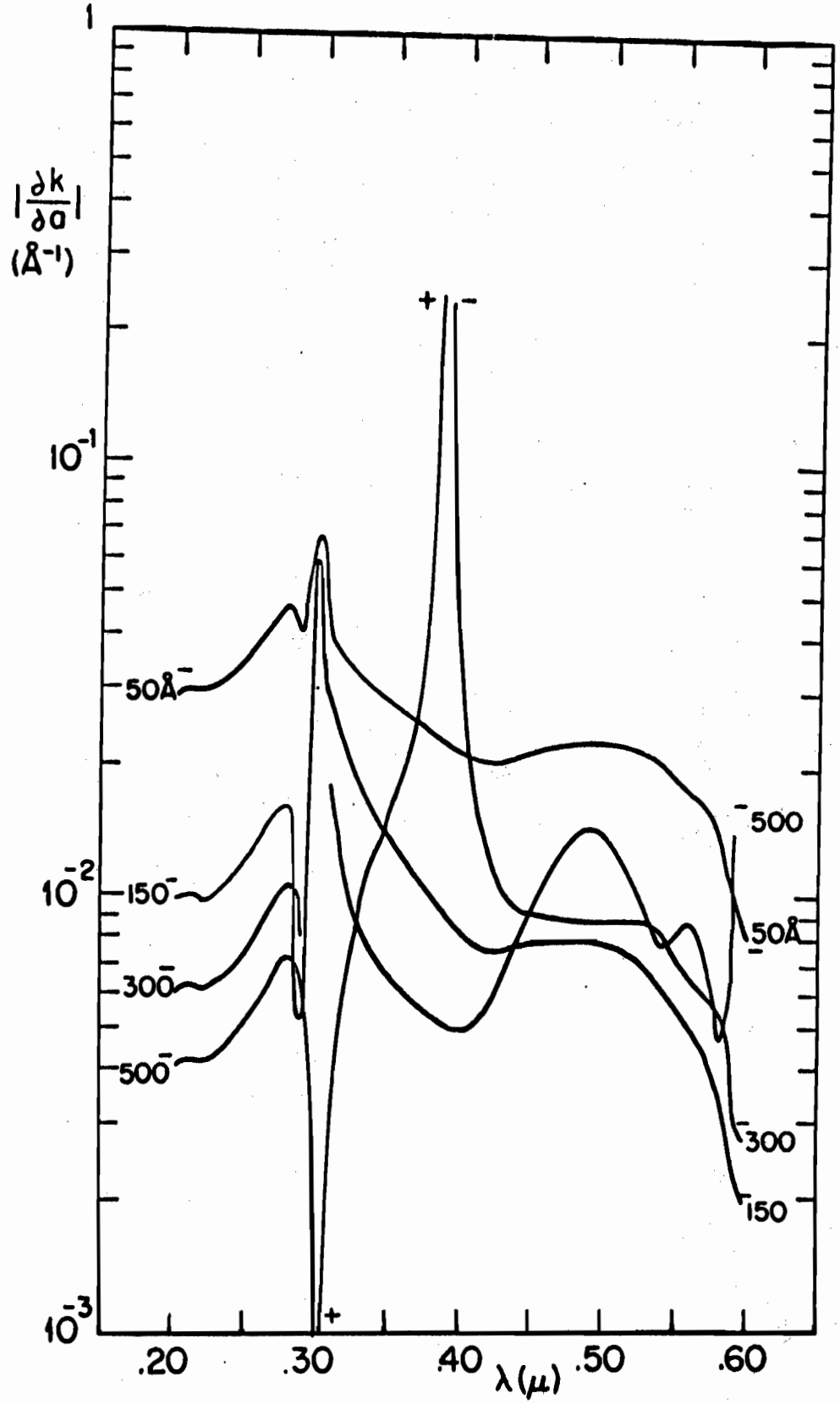

FIG. 3-12c $|\frac{\partial k}{\partial a}|$.

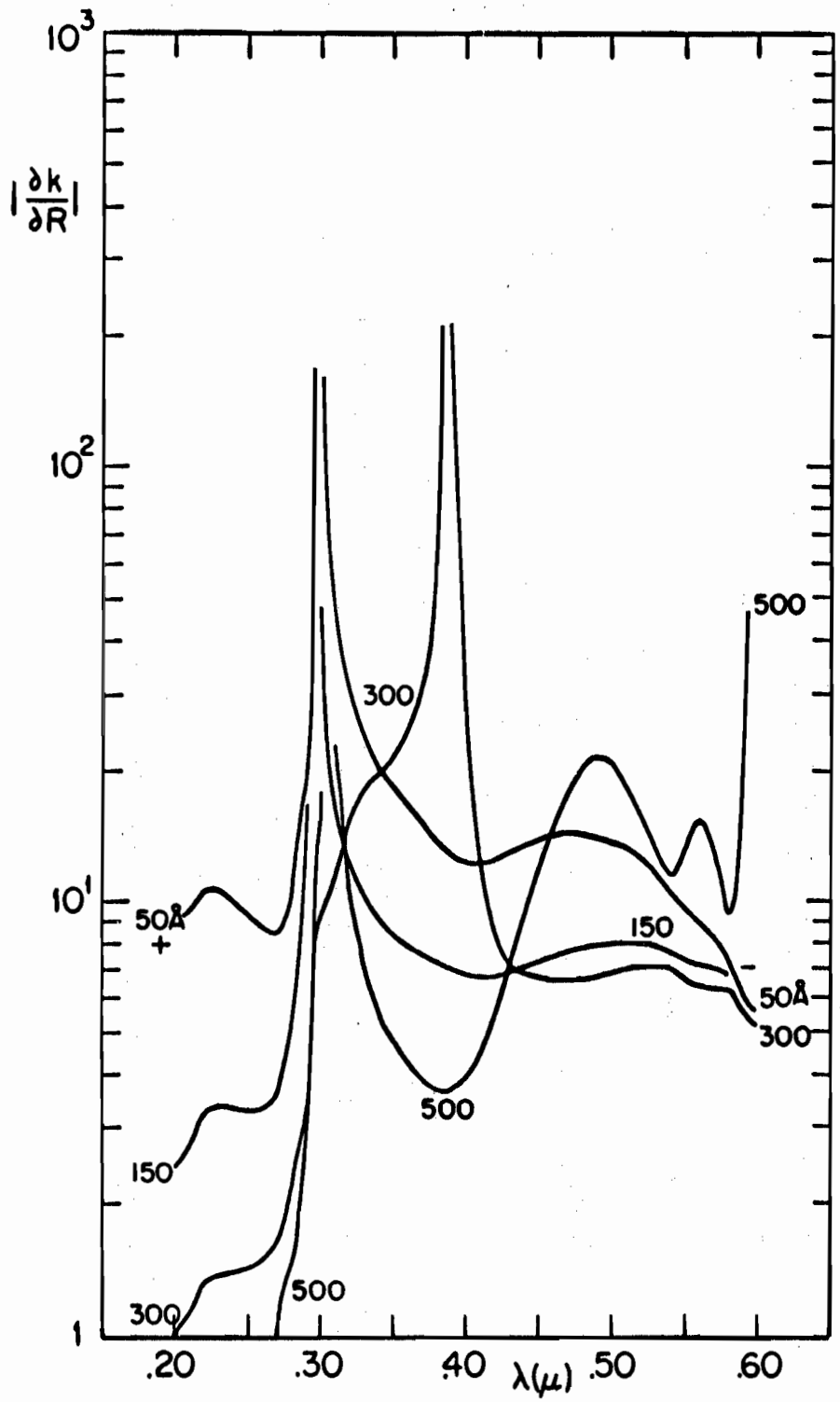

FIG. 3-12a THE EXTINCTION COEFFICIENT ERROR DERIVATIVES VS. λ FOR THE R-T MODEL OF A Ge FILM ON CaF2.

a. $\left|\frac{\partial k}{\partial R}\right|$.

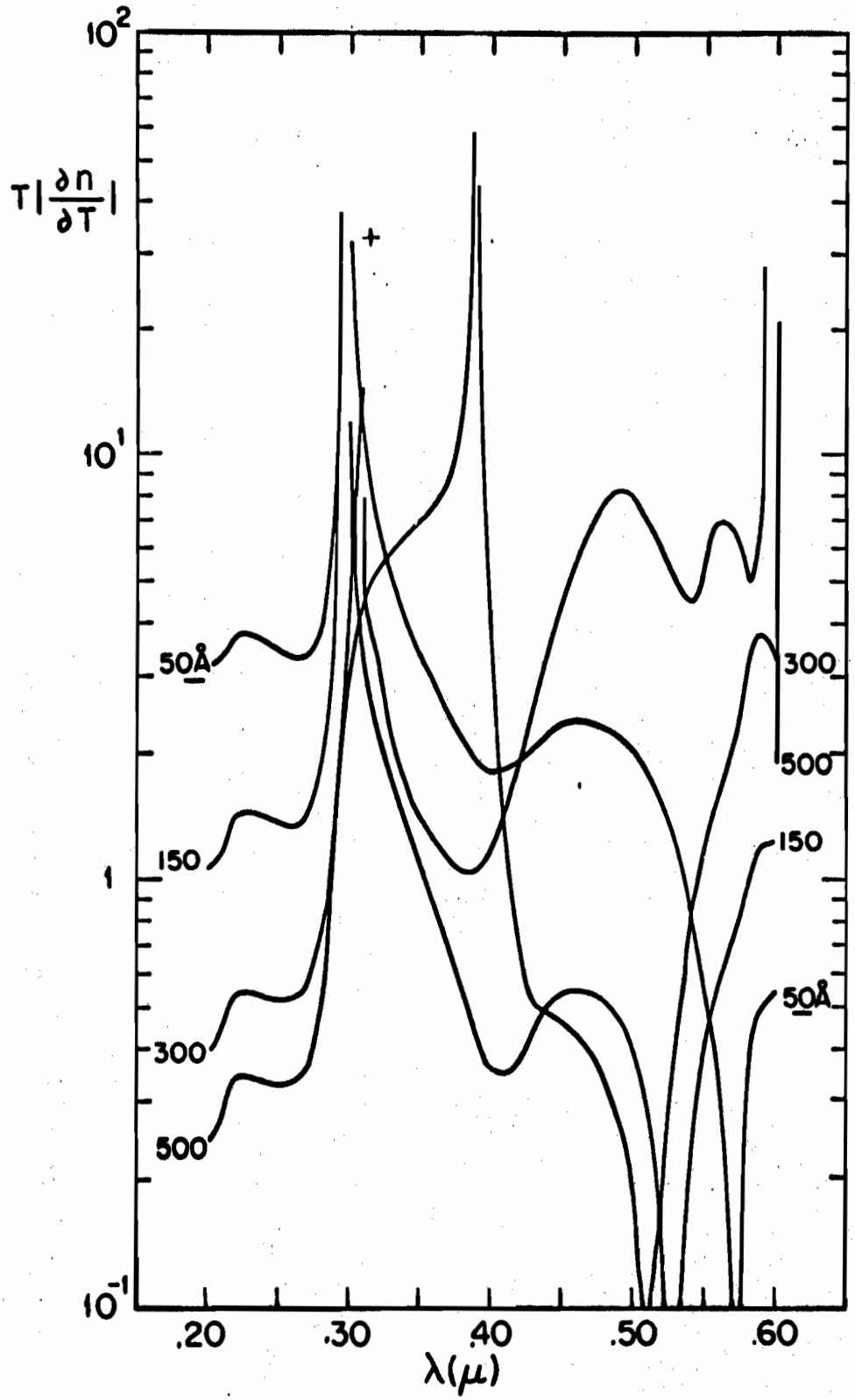

FIG. 3-11b $T\left|\frac{\partial n}{\partial T}\right|$.

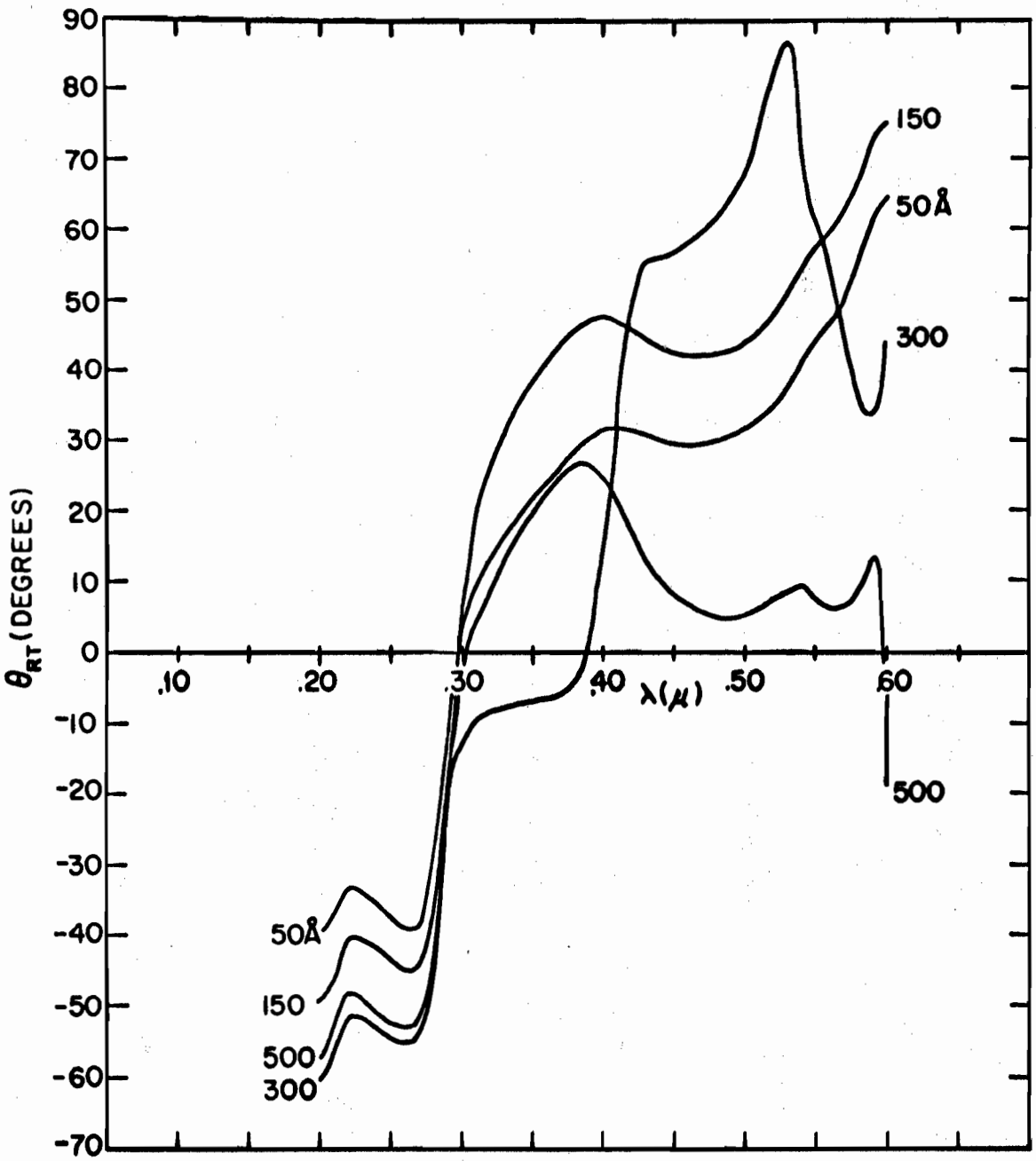

FIG. 3-10 THE ANGLE OF ROOT-LOCUS INTERSECTIONS, θ_{RT}, VS. λ FOR THE R-T MODEL OF A Ge FILM ON CaF_2. FILM THICKNESS IS INDICATED ON EACH CURVE.

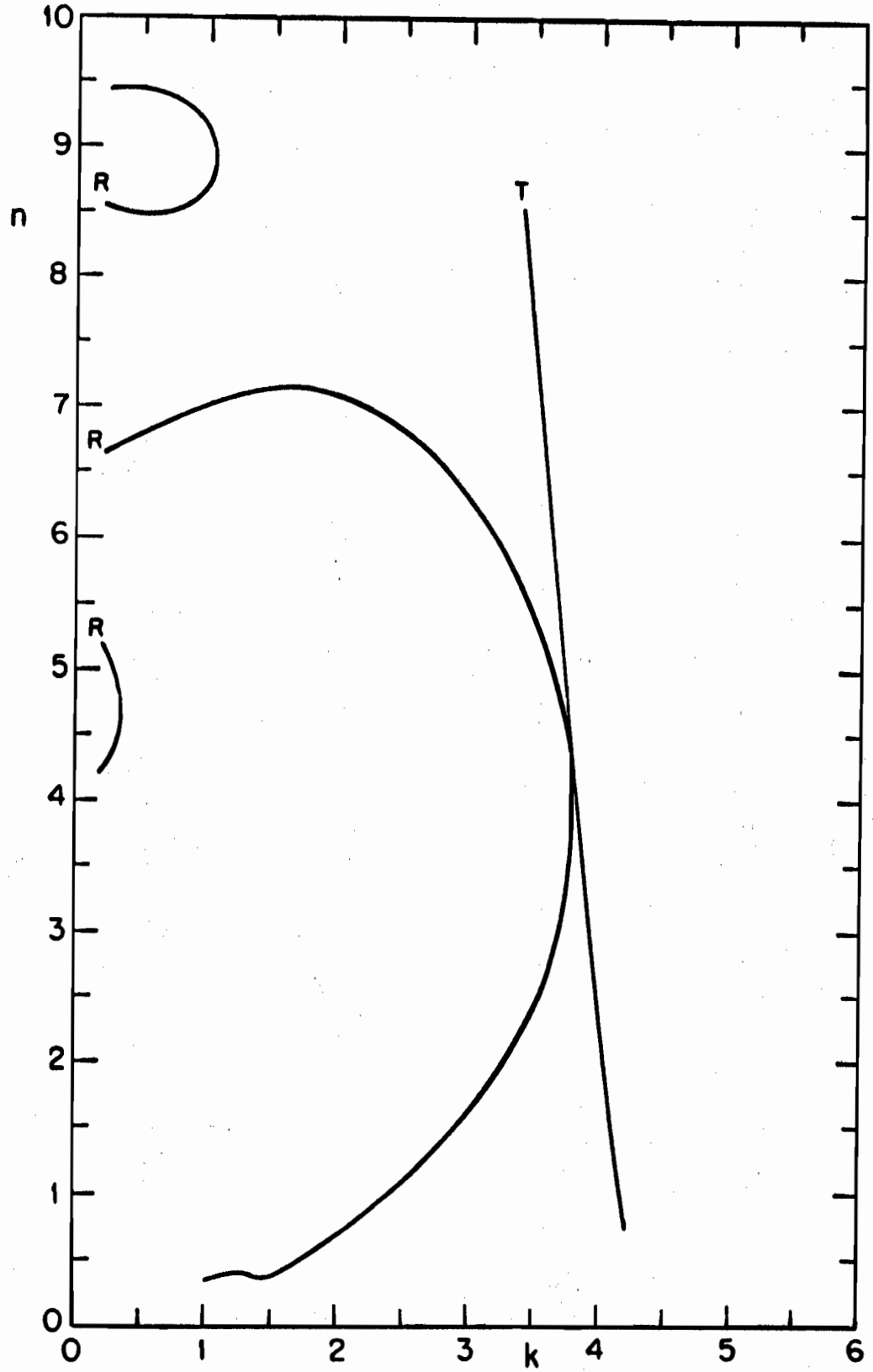

FIG. 3-9b $\lambda = 3000\text{Å}$, $a = 500\text{Å}$.

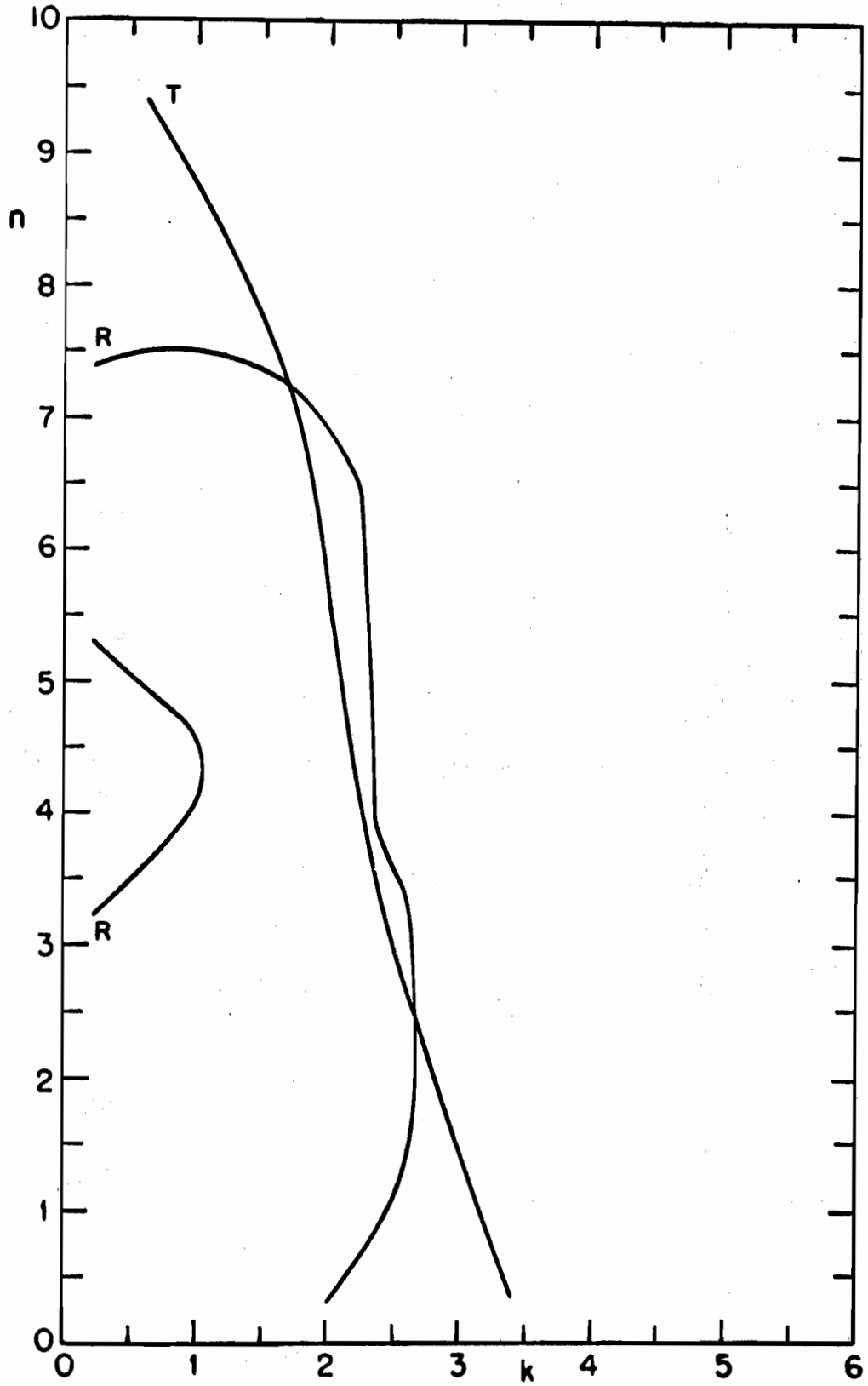

FIG. 3-8d $\lambda = 3900\text{Å}, a = 300\text{Å}$.

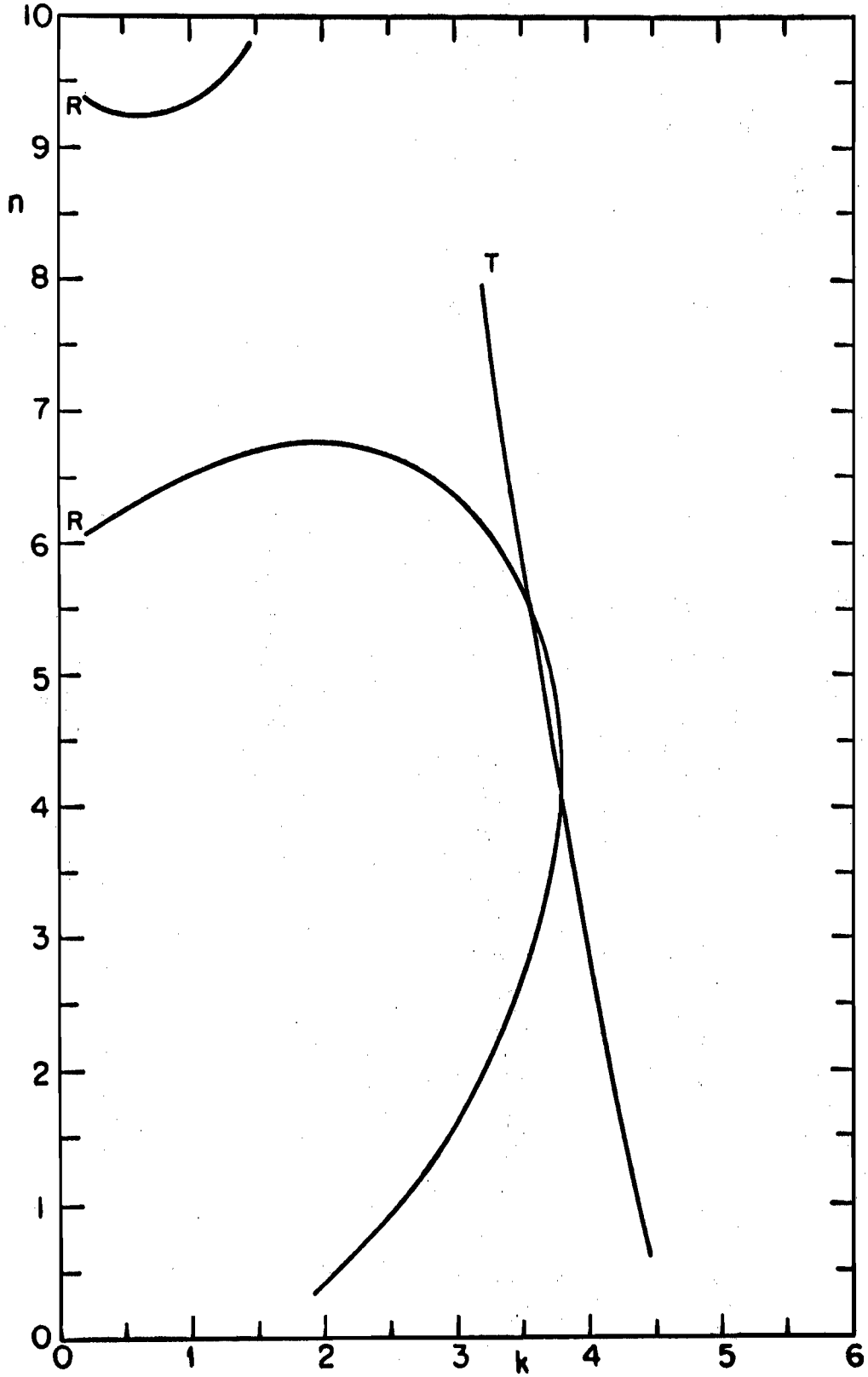

FIG. 3-8b λ = 3000Å, a = 300Å.

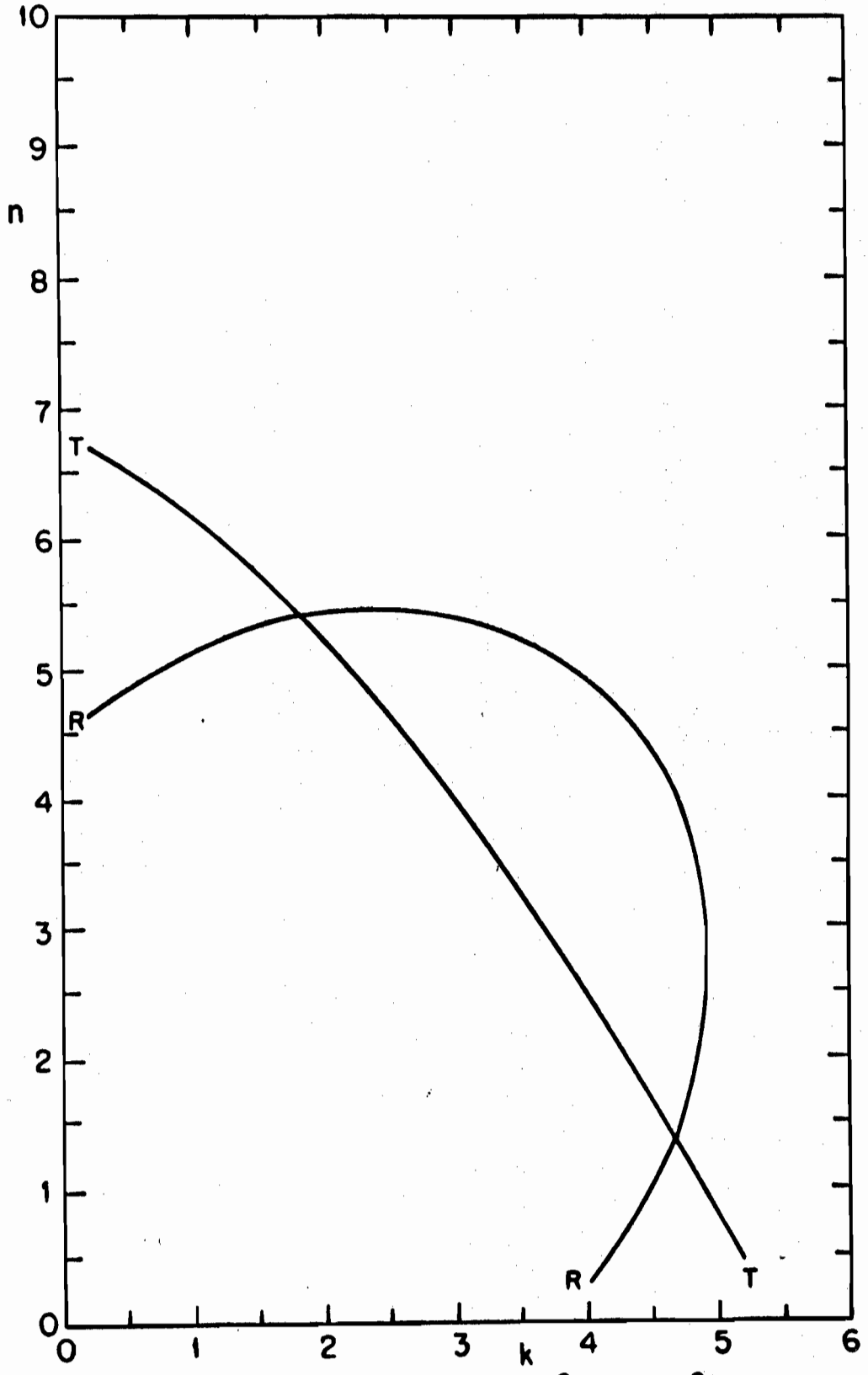

FIG. 3-7c $\lambda = 5500\text{Å}, a = 150\text{Å}$.

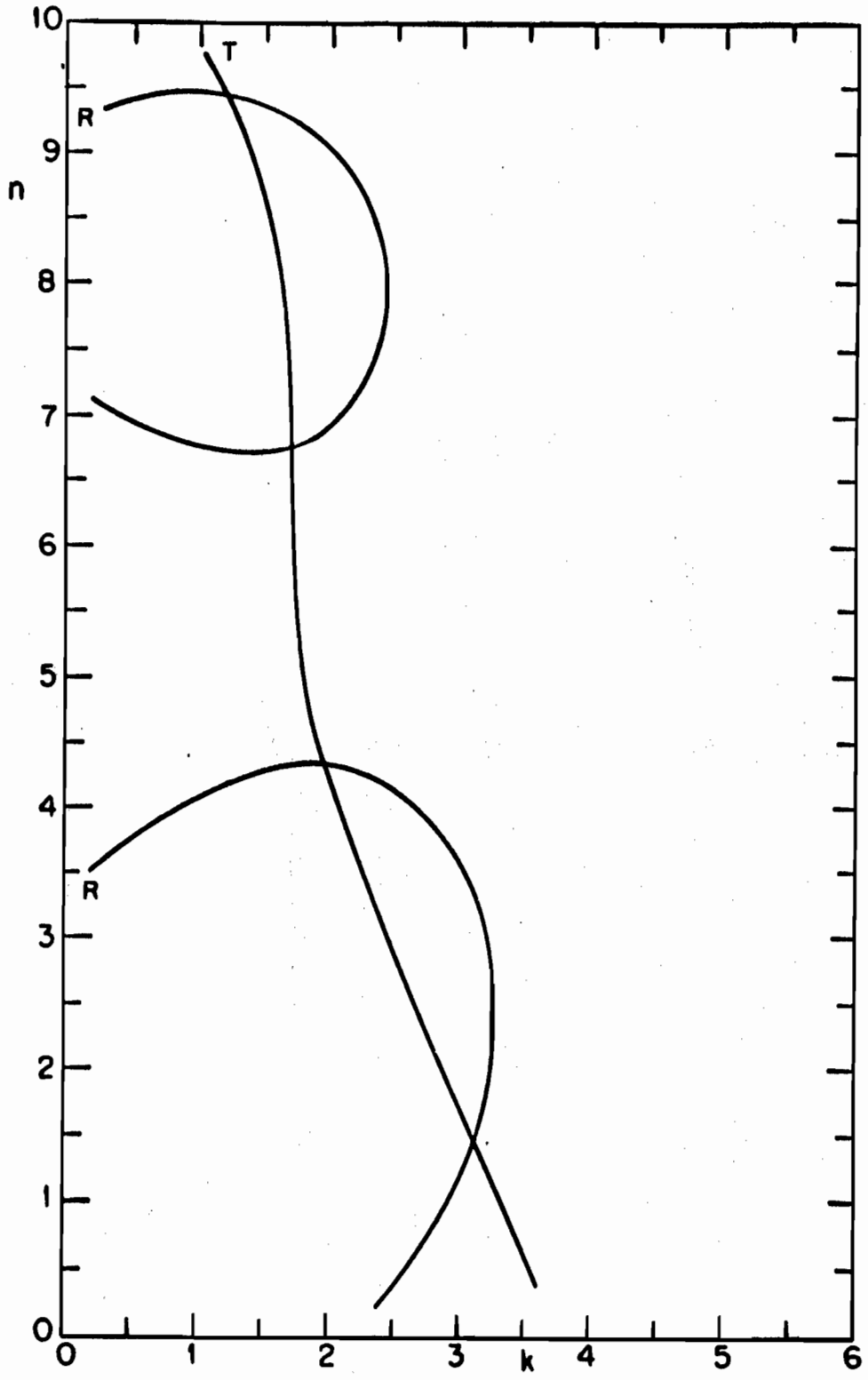

FIG. 3-7a THE ROOT-LOCUS DIAGRAM FOR THE R-T MODEL OF A 150Å Ge FILM ON CaF2. $\lambda = 2500$Å.

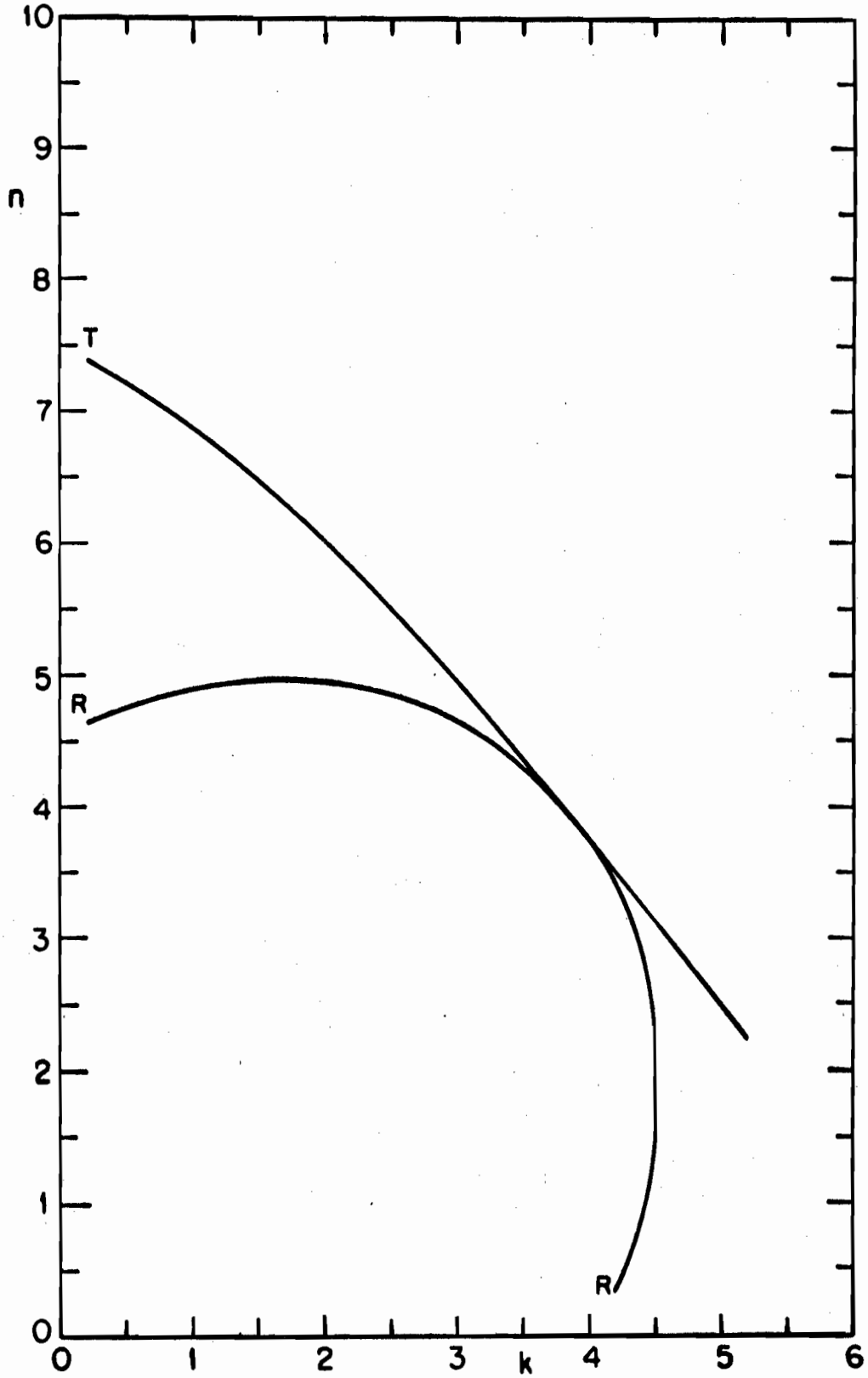

FIG. 3-6b $\lambda = 3000\text{Å}$, $a = 50\text{Å}$.

just what is predicted by the simpler model, even though $n^2 = k^2 + 1$ violates one of the assumptions of its derivation. On the other hand, that interference is not entirely without its effects is demonstrated by the 300Å film for $\lambda = 3900$Å. Here we have a condition of near tangency for $n^2 \neq k^2 + 1$.

Figures 3-10, 3-11, and 3-12 present θ_{RT} and the magnitude of the error derivatives as functions of wavelength for the four thicknesses mentioned above. These figures confirm in detail our previous discussion on the root-locus diagrams. In addition, we see that for short wavelengths the behavior is fairly independent of thickness, except for the 300Å case where the error derivative singularity is shifted to longer wavelengths. At these longer wavelengths, the effects of interference become more apparent. Note that for the complex model of equations (3-4) and (3-6), singularities can appear in all the error derivatives.

In order to gain some feeling for the wavelength ranges over which reasonable experimental errors in R, T, and a would lead to, unreasonable errors in n and k the bar diagrams Figs. 3-13, 3-14, and 3-15 were constructed. The choice of a "reasonable experimental error" is somewhat arbitrary. However, one can generally conclude that an absolute error in n and k of no greater than .5 is necessary if one is to approach the accuracy of the dispersion analysis. For

$$n = n_R(k) \tag{3-20a}$$

and for (3-19b) another:

$$n = n_T(k) \ . \tag{3-20b}$$

Equations (3-20) are curves in the n - k plane, and the points at which they intersect are the simultaneous solutions to equations (3-19). The equations (3-20) will be called the root-locus equations. The root-locus of equation (3-9a) is a circle of radius $2\sqrt{R}/(1-R)$ and center at $n = (1+R)/(1-R)$, $k = 0$. On the other hand, the root-locus of equation (3-9b) or (3-10) has no simple form. However, if the absorption is high enough, n has roughly a decaying exponential dependence on k. Let us now recall that the magnitude of the vector product of two unit vectors is equal to the sine of the angle between them. Applying this fact to equations (3-19), we obtain:

$$\sin\theta_{RT} = \left|\frac{\nabla R \times \nabla T}{|\nabla R||\nabla T|}\right| = \frac{J}{\left(\left[\left(\frac{\partial R}{\partial n}\right)^2 + \left(\frac{\partial R}{\partial k}\right)^2\right]\left[\left(\frac{\partial T}{\partial n}\right)^2 + \left(\frac{\partial T}{\partial k}\right)^2\right]\right)^{\frac{1}{2}}} \ . \tag{3-21}$$

Thus we see that when $J = 0$, $\theta_{RT} = 0$, or that curve (3-20a) ceases to intersect curve (3-20b). Instead, the two curves become tangent to each other thus leading to a highly unstable condition with regard to the dependence of the derived n and k on the experimental errors in R and T. If the errors are such as to prevent any intersection or tangency at all, then we have no real roots. This is

the vanishing of the Jacobian, and that it is this quantity we should scrutinize. Although the above formalism has been developed primarily for the more intractable film formulas, it will be instructive to examine briefly the explicit derivatives and the Jacobian for equations (3-9a) and (3-10) which are:

$$\frac{\partial R}{\partial n} = 4(n^2 - k^2 - 1)/[(1 + n)^2 + k^2]^2 \qquad (3\text{-}17a)$$

$$\frac{\partial R}{\partial k} = 8nk/[(1 + n)^2 + k^2]^2 \qquad (3\text{-}17b)$$

$$\frac{\partial T}{\partial n} = -32\, e^{-\alpha a}\, n^2(n^2 - k^2 - 1)/[(1 + n)^2 + k^2]^3 \qquad (3\text{-}17c)$$

$$\frac{\partial T}{\partial k} = -64\, e^{-\alpha a}\, n^2\left[k + \frac{\pi a}{\lambda}\,[(1+ n)^2 + k^2]\right]/[(1+ n)^2+ k^2]^3 \qquad (3\text{-}17d)$$

$$\frac{\partial R}{\partial a} = 0 \qquad (3\text{-}17e)$$

$$\frac{\partial T}{\partial a} = -\frac{64\pi n^2 k}{\lambda}\, e^{-\alpha a}/[(1 + n)^2 + k^2]^2 \qquad (3\text{-}17f)$$

$$J = -\frac{256\pi a}{\lambda}\, e^{-\alpha a}\, n^2(n^2- k^2 - 1)/[(1+n)^2+ k^2]^4 \ . \qquad (3\text{-}17g)$$

The corresponding error derivatives are:

$$\frac{\partial n}{\partial R} = \frac{\lambda k}{\pi a} + [(1+ n)^2+ k^2]\ \ [(1+ n)^2 + k^2]/4(n^2 - k^2 - 1) \qquad (3\text{-}18a)$$

$$\frac{\partial n}{\partial T} = \frac{\lambda k}{\pi a}\,[(1 + n)^2 + k^2]^2\, e^{\alpha a}/32n(n^2 - k^2 - 1) \qquad (3\text{-}18b)$$

$$\frac{\partial k}{\partial R} = -\frac{\lambda}{8\pi n a}\,[(1 + n)^2 + k^2] = -\frac{\lambda}{2\pi a(1 - R)} \qquad (3\text{-}18c)$$

$$\frac{\partial k}{\partial T} = -\frac{\lambda}{64\pi n^2 a}\,[(1+ n)^2+ k^2]^2\, e^{\alpha a} = -\frac{\lambda}{4\pi a T} \qquad (3\text{-}18d)$$

possible. If we examine the germanium optical constant curves of Figs. 1-3b we see that equation (3-13) is satisfied near $\lambda = 3000\text{Å}$, and that the T vs. R representation plot shown in Fig. 3-5 for a 300Å film indicates that near this wavelength small changes in the experimental values of R and T may determine whether or not n is real. We might add that the equivalent to (3-13) for the dielectric constant $\tilde{\epsilon}$ is $\epsilon_1 = 1$ and $\epsilon_2 = 2k\sqrt{k^2 + 1}$.

2. The First Order Error Derivatives for Germanium Thin Films.

In general, we are not able to obtain n and k in terms of R and T explicitly as we did in equations (3-11), and some sort of numerical operations must be performed in order to find the optical constants. However, regardless of the numerical procedure actually used, we shall want to know in principle how experimental errors in R and T affect the error in the derived optical constants. Therefore, we write the following equations in terms of the first-order error differentials:

$$dn = \frac{\partial n}{\partial R} dR + \frac{\partial n}{\partial T} dT + \frac{\partial n}{\partial a} da \qquad (3\text{-}14a)$$

$$dk = \frac{\partial k}{\partial R} dR + \frac{\partial k}{\partial T} dT + \frac{\partial k}{\partial a} da \ . \qquad (3\text{-}14b)$$

It is to be remembered that in the mathematical context of the problem we treat R and T as the dependent variables, n and k as the independent variables, and a and λ as parameters. Now, because

We shall now state two important approximations to equations (3-4) in order to discuss qualitatively some of the results to be derived numerically and empirically from these equations. In doing this, the presence of the substrate backing will be neglected completely as it has no importance in any qualitative discussions. Equations (3-4a) and (3-4c) become, respectively:

$$R = R^N \frac{\left(e^{\frac{\alpha a}{2}} - e^{-\frac{\alpha a}{2}}\right)^2 + 4\sin^2\varphi}{\left(e^{\frac{\alpha a}{2}} - R^N e^{-\frac{\alpha a}{2}}\right)^2 + 4R^N \sin^2(\varphi + \psi)} \tag{3-8a}$$

$$T = \frac{16(n^2 + k^2)}{[(1+n)^2 + k^2]^2}$$

$$\times \frac{1}{\left(e^{\frac{\alpha a}{2}} - R^N e^{-\frac{\alpha a}{2}}\right)^2 + 4R^N \sin^2(\varphi + \psi)} \tag{3-8b}$$

where R^N, ψ, φ, and α are given by equations (3-4d), (3-4f), (3-4i), and (3-4h), respectively. One important approximation deals with the case of very strong absorption where the absorption damps out interference effects. This is the case where k is of the order of n and $e^{\alpha a} \gg 4$. In the wavelength region below 3500Å for a 300Å germanium film, this is a very good approximation. Applying these considerations yields:

$$R = R^N = \frac{(1 - n)^2 + k^2}{(1 + n)^2 + k^2} \tag{3-9a}$$

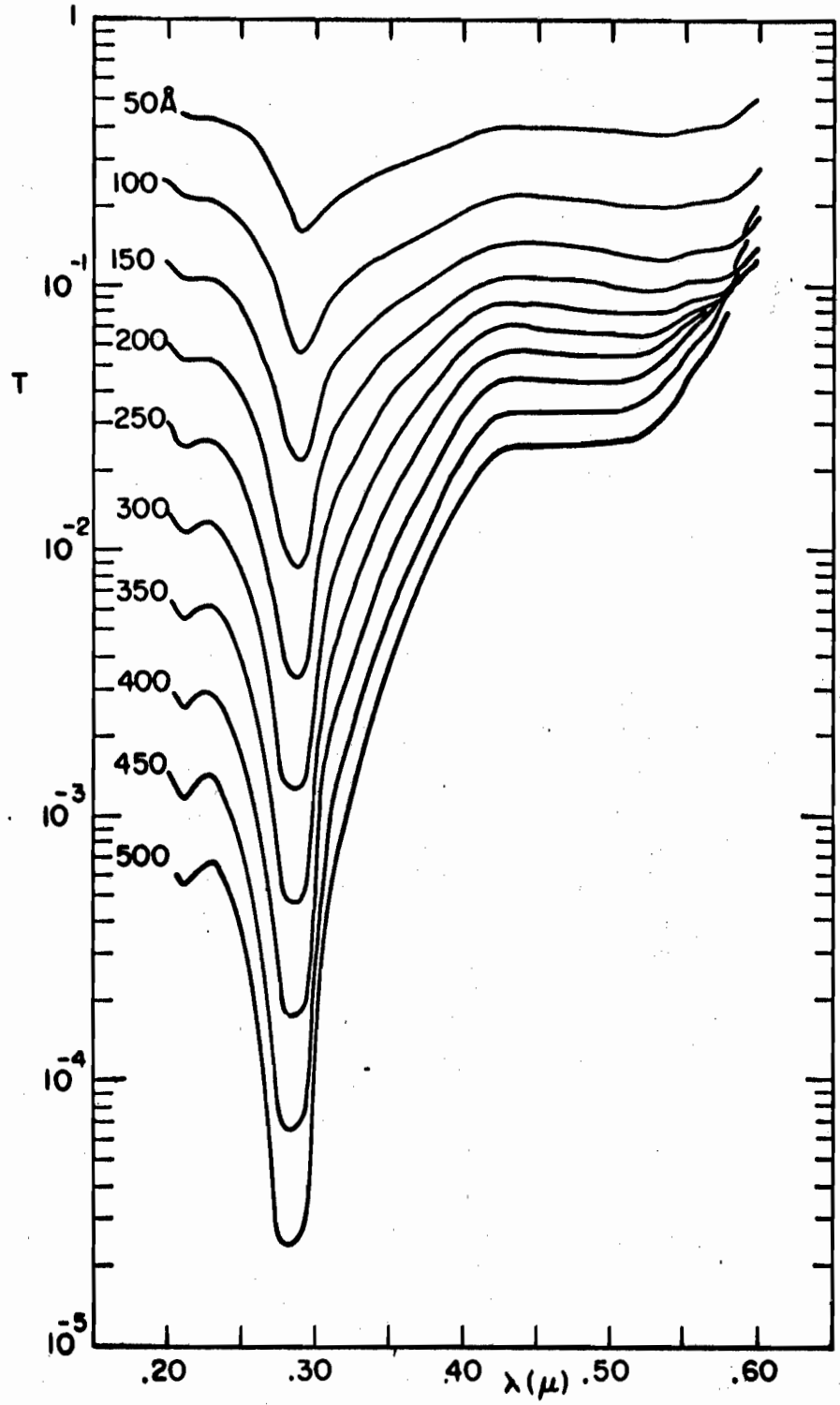

FIG. 3-3 THE TRANSMISSION OF GERMANIUM THIN FILMS ON CaF_2 SUBSTRATES USING THE OPTICAL CONSTANTS DERIVED BY PHILIPP(2). THE FILM THICKNESS IS INDICATED FOR EACH CURVE.

$$T = T_{FS}(1 - R_{AS}) + T_{FS}\, R_{AS}\, R_{FS}(1 - R_{AS}) + T_{FS}\, R_{AS}\, R_{FS}\, R_{AS}\, R_{FS}(1 - R_{AS}) + \cdots$$

or

$$T = \frac{T_{FS}(1 - R_{AS})}{1 - R_{AS}\, R_{FS}} \tag{3-6b}$$

where

$$R_{AS} = \frac{(1 - n_s)^2}{(1 + n_s)^2} . \tag{3-7}$$

For the materials studied in this work, we may put typically for the purpose of ascertaining the degree to which the finite substrate correction influences the results $T_{FS} = 10^{-1}$, $R_{FS} = .50$, $R_{AS} = .03$. We then have an additive factor of $3 \cdot 10^{-4}$ to the reflectivity R and the multiplicative factor .97 to the transmissivity T. Only the factor for T can possibly be expected to amount to anything greater than the experimental error; however, since the inclusion of the finite substrate effect does not complicate any of the analysis to follow, we will keep it for the sake of completeness.

Figure 1-3b shows the optical constants of germanium derived by Philipp [2]. The result of substituting these constants into equations (3-6) is given for T in Fig. 3-3 and for R in Fig. 3-4. The curves are calculated for films ranging in thickness from 50Å to 500Å in intervals of 50Å . This covers the usable thickness range in which one can perform transmission experiments. These curves prove to be invaluable for planning experiments and for quickly interpreting the measurements.

$$R_{FS}^{N} = \frac{(n_s - n)^2 + k^2}{(n_s + n)^2 + k^2} \tag{3-4e}$$

$$\psi_{FA} = \tan^{-1} \frac{2k}{n^2 + k^2 - 1} \tag{3-4f}$$

$$\psi_{FS} = \tan^{-1} \frac{2n_s k}{n^2 + k^2 - n_s^2} \tag{3-4g}$$

$$\alpha = \frac{4\pi k}{\lambda} \tag{3-4h}$$

$$\varphi = \frac{2\pi na}{\lambda} \, . \tag{3-4i}$$

This is the form usually found in the literature [4, 6]. An even more explicit form is that derived by Harris and Loeb [5]†:

$$R_{FA} = \frac{\left| \tilde{n}(1 - n_s) \cos \frac{2\pi\tilde{n}a}{\lambda} - i(n_s - \tilde{n}^2) \sin \frac{2\pi\tilde{n}a}{\lambda} \right|^2}{\left| \tilde{n}(1 + n_s) \cos \frac{2\pi\tilde{n}a}{\lambda} - i(n_s + \tilde{n}^2) \sin \frac{2\pi\tilde{n}a}{\lambda} \right|^2} \tag{3-5a}$$

$$R_{FS} = \frac{\left| \tilde{n}(n_s - 1) \cos \frac{2\pi\tilde{n}a}{\lambda} - i(n_s - \tilde{n}^2) \sin \frac{2\pi\tilde{n}a}{\lambda} \right|^2}{\left| \tilde{n}(1 + n_s) \cos \frac{2\pi\tilde{n}a}{\lambda} - i(n_s + \tilde{n}^2) \sin \frac{2\pi\tilde{n}a}{\lambda} \right|^2} \tag{3-5b}$$

$$T_{FS} = \frac{4 n_s |\tilde{n}|^2}{\left| \tilde{n}(1 + n_s) \cos \frac{2\pi\tilde{n}a}{\lambda} - i(n_s + \tilde{n}^2) \sin \frac{2\pi\tilde{n}a}{\lambda} \right|^2} \, . \tag{3-5c}$$

---

†It should be pointed out that the denominator of equation (4) of reference [5] contains a rather obvious sign error.

$$r_{FS} = \frac{\rho_{FS} + \rho_{AF}\, e^{+2i\tilde{k}_F a}}{1 + \rho_{FA}\,\rho_{SF}\, e^{+2i\tilde{k}_F a}} \tag{3-1b}$$

$$t_{FS} = \frac{\tau_{FS}\,\tau_{AF}\, e^{+i\tilde{k}_F a}}{1 + \rho_{FA}\,\rho_{SF}\, e^{+2i\tilde{k}_F a}} \tag{3-1c}$$

$$t_{SF} = \frac{\tau_{FA}\,\tau_{SF}\, e^{+i\tilde{k}_F a}}{1 + \rho_{FS}\,\rho_{SF}\, e^{+2i\tilde{k}_F a}} = \frac{(\tilde{n})^2}{n_s}\, t_{FS} \tag{3-1d}$$

where we have made use of the following results of Chapter One, Section B-1:

$$\rho_{FA} = \frac{1 - \tilde{n}}{1 + \tilde{n}} = -\rho_{AF} \tag{3-2a}$$

$$\rho_{SF} = \frac{\tilde{n} - n_s}{\tilde{n} + n_s} = -\rho_{FS} \tag{3-2b}$$

$$\tau_{FS} = \frac{2\tilde{n}}{\tilde{n} + n_s} = \frac{\tilde{n}}{n_s}\,\tau_{SF} \tag{3-2c}$$

$$\tau_{AF} = \frac{1}{1 + \tilde{n}} = \frac{1}{\tilde{n}}\,\tau_{FA} \tag{3-2d}$$

$$\tau_{FS} - \rho_{SF} = 1 \tag{3-2e}$$

$$\tau_{AF} - \rho_{FA} = 1 \quad . \tag{3-2f}$$

From equations (1-16a) and (1-23) we obtain the following rules for the intensity reflectivity and transmissivity coefficients of the model in Fig 3-1.

[15] R. L. Schalla, L. H. Thaller, and A. E. Potter, Jr., J. Appl. Phys. 33, 2554 (1962).

[16] A. L. Pundsack, J. Appl. Phys. 34, 2306 (1963).

[17] C. S. Barrett, Structure of Metals (McGraw-Hill, New York 1952).

[18] Z. G. Pinsker, Electron Diffraction (Butterworths, London, 1953).

[19] B. W. Sloope and C. O. Tiller, Japan. J. Appl. Phys. 2, 308 (1963).

[20] B. W. Sloope and C. O. Tiller, J. Appl. Phys. 32, 1331 (1961).

[21] R. S. Sennett and G. D. Scott, J. Opt. Soc. Am. 40, 203 (1950).

[22] H. G. F. Wilsdorf, Bull. Am. Phys. Soc. 10, 342 (1965).

[23] O. S. Heavens, see reference 22 of Chapter One.

[24] M. Cardona, Technical Report No. HP-5, Gordon McKay Laboratory of Applied Science, Harvard University, 1959 (unpublished). See Fig. 6-8.

[25] C. Salzberg and J. Villa, J. Opt. Soc. Am. 48, 579 (1958).

particularly when the height of the aggregates approaches the average film thickness. When the mean thickness is only a few dozen atoms, the picture of a film as an isotropic, homogeneous, plane parallel-sided layer is no longer valid. Hence, any reference to "film thickness" will always imply some sort of average thickness.

We used simply the infrared transmission of the film to obtain its thickness. In this region $k = 0$, and because the films are epitaxial, the bulk refractive index can be used with a high degree of confidence. The index of refraction of bulk single crystal germanium has been measured by Cardona in the wavelength region 1.8μ to 5.5μ [24], and there is evidence that these values hold also for polycrystalline germanium [25]. We measured the transmission at 1.8μ and 2.0μ, used Cardona's values for n, and inverted equation (3-6b) to find the thickness. Measurements were made at several different positions on the film surface and the results averaged. (The rms deviation was usually about 10Å to 20Å). Fortunately, the transmission varied quite rapidly over the thickness range of interest -- the films were much too thin for interference fringe methods -- so that the thickness to transmission variation was about 10Å /% with T being measurable to within one percent. We feel that this method gave satisfactory results.

and roughness. However, we should point out that, to date, no one has claimed to make a smooth epitaxial film of germanium on CaF_2.

The effect of ambient pressure on the surface topography and crystallinity of the films has not been extensively studied and those results that have been reported seem to be in conflict. Catlin, et al. [14], report that ambient pressures of 10^{-9} torr allow epitaxial deposition at lower substrate temperatures for a given deposition rate than had been previously observed. Conversely, it has also been reported that a poor vacuum enhances epitaxy [22].

Figure 2-7 is a photomicrograph of the surface of one of our films. The dark area is the substrate and the speckled area is the germanium film. Dark field illumination was used to bring out the surface detail. This film was grown at a substrate temperature of about 700°C and with a deposition rate around 100Å / min; that is, under conditions favorable for the formation of a rough growth. To the casual observer, the film looks quite shiny; however, more intensive investigation reveals the effect discussed in Section A-4. It is hard to estimate the size of the aggregates from Fig. 2-7 alone, but they appear to be at least a few thousand Å in width. The height is even more difficult to resolve. Sloope [19] indicates that for some films the thickness variation may be

obtain the spot and ring patterns typical of Figs. 4-6 and 4-8. That this is so, can be seen by imagining the projection pattern caused by randomly rotating the reciprocal lattice about the ⟨111⟩ direction and noting the various intersections with the Ewald plane. In addition, if we randomly rotate the reciprocal lattice in all possible directions, including ⟨111⟩, we will generate the well-known ring pattern common to powder x-ray diffraction analysis.

In Fig. 2-6, we have a sequence of RED patterns showing various stages in the growth of the epitaxial film. These were made with the Via apparatus described above during the initial period of this research. We see that the start of epitaxy is immediate and continues throughout the growth of the film. The substrate pattern is rather obscure because CaF_2 is a dielectric and tends to become charged and repel the incident electron beam. The sudden appearance of the germanium Laue pattern when the substrate is exposed to the germanium vapor stream is probably due to the rapid development of nucleations on the crystal substrate surface. As the film grows and becomes more or less continuous, the Laue pattern spots should become slightly elongated. Figure 2-6 indicates that this is the case. The elongation may be attributed to a refractive shift of the pattern caused by some sort of wavy surface on a thin layer of finite thickness, whereas the sharp spots are caused by transmission through discrete nucleations. This

intercept the reflected beams we will obtain the well-known Laue pattern. For the very high energy electron beams that are used for RED, the wave vector of the beam becomes very much longer than the distance between points of the reciprocal lattice. For example, the magnitude of a 75 kV electron beam is about 100 times greater than the reciprocal lattice constant of germanium. Therefore, with respect to any given portion of the reciprocal lattice, the Ewald sphere may be considered a plane. This means that for an electron beam incident along a symmetry direction there will appear on the film a projection of the reciprocal lattice points lying in the plane normal to this direction. In the RED technique, the incident electron beam strikes the surface of the sample at a glancing angle and penetrates only a small distance normal to the surface before undergoing reflection. However, the total path traveled in the crystal is much greater than this depth; therefore, because of this fact and the very small angle of incidence it is possible to discuss RED patterns as actually transmission diffractograms.

Figure 2-6 shows the RED pattern for an epitaxial Ge film whose surface vector is of the ⟨111⟩ type with the electron beam incident in a ⟨110⟩ type direction. If one had a polycrystalline film whose surface vector was mainly ⟨111⟩ but whose azimuthal vectors were randomly distributed among the individual crystallites, one would

TABLE 2-1

The pertinent physical properties of possible substrate materials suitable for the epitaxial deposition of germanium films.

Material	Lattice Configuration†	Lattice Constant (Å)†	Melting Point (°C)‡	Thermal Expansion ($°C^{-1}$)‡	UV Cutoff (Å)‡
Ge	O_h^7	5.647	910 ††	$5.8 \cdot 10^{-6}$ (0°C) ††	—
CaF_2	O_h^5	5.451	1360	$24 \cdot 10^{-6}$ (20°C-60°C)	1250
BaF_2	O_h^5	6.184	1320	$18 \cdot 10^{-6}$ (0°C-300°C)	1300
SrF_2	O_h^5	5.86	1400		1200
LiF	O_h^5	4.01	848	$37 \cdot 10^{-6}$ (0°C-200°C)	1040
KC	O_h^5	6.28	776	$36 \cdot 10^{-6}$ (20°C-60°C)	2000
KBr	O_h^5	6.578	730	$43 \cdot 10^{-6}$ (20°C-60°C)	2300
NaF	O_h^5	4.62	997	$36 \cdot 10^{-6}$ (25°C)	1900
NaCl	O_h^5	5.627	801	$44 \cdot 10^{-6}$ (-50°C-200°C)	2000

† See reference 8.

‡ See reference 9.

†† See reference 10.

to temperature as fast as the thermal inertia of the heater would allow. For epitaxy to result, the temperature would have to exceed 550°C as read by the substrate thermocouple. During this time there would be little or no rise in pressure. The substrate would then undergo bake-out for a short period, usually 15 minutes to an hour. The source would next be heated to an appropriate level to produce a desired deposition rate. This could be estimated by observing the darkening of a monitor microscope slide at the same distance from the source as the substrate. The power dissipation of the source and substrate heaters was recorded in order to maintain resetability. When the desired evaporation rate was reached, the shutter shown in Fig. 2-2 was opened by means of a rotary mechanical feedthru in the vacuum system baseplate. The shutter remained opened for a predetermined time interval before being closed. Then the source heater would be shut down and the film would be given a short 5-minute post-anneal treatment at its formation temperature before being cooled. During the evaporation, the pressure would usually rise to 1 to $3 \cdot 10^{-6}$ torr. The procedure described above, with minor variations, was the one used to produce the films from which the optical data reported in this work were taken.

3. The Harvard Apparatus. Deposition Procedures.

The first epitaxial films of germanium on CaF_2 were made by Via and Thun [11] and Marucchi and Nifontoff [12]. The most extensive investigation to date into the formation conditions and structure of this film-substrate system has been done by Sloope and Tiller [13], although several other works have also been reported [14-16]. In each of these efforts, essentially the same technique was used that is about to be discussed here in conjunction with our work. What will be referred to as the Harvard apparatus has actually undergone a continuous evolution during the course of this work. The changes made were not in technique but were rather improvements in the convenience of operation. Hence, for purposes of general discussion we will refer to the schematic of Fig. 2-1. The actual apparatus is shown in Fig. 2-2 with the components relating to Fig. 2-1 designated therein.

The substrate is mounted on a .020 inch Ta plate with .005 inch Ta spring clips. This assembly is then heated by placing it under a series of .015 inch diameter Ta wire heater coils. Figure 2-3 shows the actual substrate holder with a piece of CaF_2 in place. The substrate temperature was measured by holding a Pt-Pt 10% Rh thermocouple on the substrate surface with one of the Ta clips as indicated in Fig. 2-3. The Ta heater coils were energized electrically from outside the vacuum chamber where the current flow, hence temperature, was regulated.

and then polishing both sides by the usual technique for preparing optical flats. Films deposited on such substrates were found to be of good crystalline quality but of very poor optical quality. Microscopic examination of these polished substrates showed that although they appeared highly polished to the naked eye they invariably possessed a surface roughness comparable in size to the final grit that was used in the polishing operation. This roughness had a highly degrading effect on the ultraviolet optical properties of a film deposited thereon (see Chapter Four for additional information). It appears as if crystalline materials with highly ionic bonds cannot be polished by conventional methods. We therefore decided to use cleaved slabs as our substrate medium. Although these substrate surfaces are rough macroscopically due to the presence of many cleavage steps, they are smooth microscopically on the exposed atomic planes. The cleavage steps cause at the most a constant error in the optical response of the film which can be minimized by carefully aligning the sample in the optical apparatus (see Chapter Four). The cleavage operation is performed by holding the block firmly in suitably jigging, aligning a razor blade parallel to the cleavage plane at the required point along the length of the crystal, and striking it sharply with a small hammer. Sometimes several attempts were required

The space group O_h^5, common to the alkali-alkaline earth halides, is of two types. For the alkali halides we have the so-called NaCl structure, while for the alkaline earth halides we have the CaF_2 structure. The CaF_2 structure is the same as the diamond structure, except that now the empty quarter-diagonal positions of the latter are occupied in the former. Both structures are suitable for the epitaxial growth of germanium; however, because the CaF_2 structure has a {111} type cleavage which is the natural direction of growth for germanium, it is slightly more preferable than the NaCl structure which has a {100} type cleavage.

(b) As the germanium bond is non-ionic in character, a reasonable match of its lattice constant to that of the substrate is to be demanded. Just how close we have to be can only be found by experiment; however, other considerations being equal, the closer we can come, the better.

(c) Because the substrate must be heated, it must be able to withstand the temperature necessary for epitaxial growth without undue deterioration. Since this temperature runs between 500° and 700°C, the melting point of the substrate should be considerably above this range. Unfortunately, many of the alkali-halides undergo appreciable evaporation well before their melting points.

(d) Again because the substrate must be heated, its linear thermal expansion coefficient becomes an important parameter.

substrate that can be tolerated. For example, it is far easier to obtain epitaxial growth of the alkali-halides than of germanium.

(c) The film grows by the formation of discrete nuclei with the bulk lattice structure which are scattered over the substrate surface. The growth continues by the enlargement of these nuclei until they grow together forming a more or less homogeneous film [3].

At present, three techniques are used to produce epitaxial films. These are vapor deposition, cathodic sputtering and vacuum deposition. Vapor deposition involves a chemical reaction between an appropriate substrate and a gas atmosphere containing a compound of the material to be deposited as a film. One of the more popular methods uses the breakdown of a halide gas of Ge or Si at the surface of a substrate of similar material [5]. This technique works well when the film-substrate system is among the group 4 or 3-5 semiconductors. As mentioned before, cathodic sputtering is making a comeback as a means of producing epitaxial films [6]; however, the predominant method is still vacuum deposition. The only major change in this method that has occurred since the pre-epitaxial era has been to heat the substrate. It has been successful for a very large number of materials besides semiconductors [7].

Chapter Two

THIN FILM FABRICATION

A. REVIEW OF METHODS OF FABRICATING THIN GERMANIUM FILMS

1. Pre-Epitaxial Methods.

The development of methods for the production of thin films for optical studies prior to the pre-epitaxial period is discussed by Heavens [1] and Holland [2]. These methods, which have much in common with post-epitaxial methods, consist of primarily three techniques, which, listed in their historical order, are electrolytic deposition, cathodic sputtering, and vacuum deposition.

Let us first, however, define precisely what we mean by the term "epitaxial." An epitaxial film is one whose azimuthal orientation and normal direction of that crystallographic plane which lies parallel to the substrate surface is congruent to the same crystallographic plane in the substrate. For example, if one has a slab of CaF_2, whose crystal symmetry is cubic, in which the surface crystallographic plane is of the {111} family with a ⟨111⟩ type direction normal to the surface and ⟨110⟩ and ⟨211⟩ type directions lying in the surface, the crystallographic orientation of a germanium film grown epitaxially on such a surface will be defined by these exact same indices. Sometimes the term "single crystal" instead of epitaxial is used; however, in view of the

Chapter One

BIBLIOGRAPHY

[1] F. Stern, Elementary Theory of the Optical Properties of Solids, Solid State Physics, vol. 15, ed. by F. Seitz and D. Turnbull (Academic Press, New York, 1963).

[2] R. W. Ditchburn, Light (Interscience Publishers Inc., New York, 1953), Fig. 15.1, p. 444.

[3] T. M. Donovan, E. J. Ashley, and H. E. Bennett, J. Opt. Soc. Am. 53, 1403 (1963).

[4] H. R. Philipp and E. A. Taft, Phys. Rev. 113, 1002 (1959).

[5] J. Tauc and A. Abraham, Proceedings of the International Conference on Semiconductor Physics, Prague, 1960 (Czechoslovakian Academy of Sciences, Prague, 1961), p. 375; J. Phys. Chem. Solids 20, 190 (1961).

[6] H. R. Philipp, private communication, Nov. 16, 1964.

[7] H. M. O'Bryan, J. Opt. Soc. Am. 26, 122 (1936).

[8] W. H. Brattain and H. B. Briggs, Phys. Rev. 75, 1705 (1949).

[9] H. A. Gebbie, Ph.D. Thesis, Reading, 1952 (unpublished), according to [10].

[10] F. Lukes, Czech. J. Phys. B10, 59 (1960).

[11] P. Nozières and D. Pines, Phys. Rev. 109, 762 (1958); Il Nuovo Cimento 9, 470 (1958).

[12] H. Ehrenreich and M. H. Cohen, Phys. Rev. 115, 786 (1959); H. R. Philipp and H. Ehrenreich, Phys. Rev. 129, 1550 (1963).

[13] C. Kittel, Introduction to Solid State Physics (Wiley, New York, 1956).

[14] J. C. Phillips and L. Kleinman, Phys. Rev. 116, 287 (1959); for a concise discussion of the pseudo-potential method, see R. Zallen, Technical Report No. HP-12, Gordon McKay Laboratory of Applied Science, Harvard University, 1964 (unpublished).

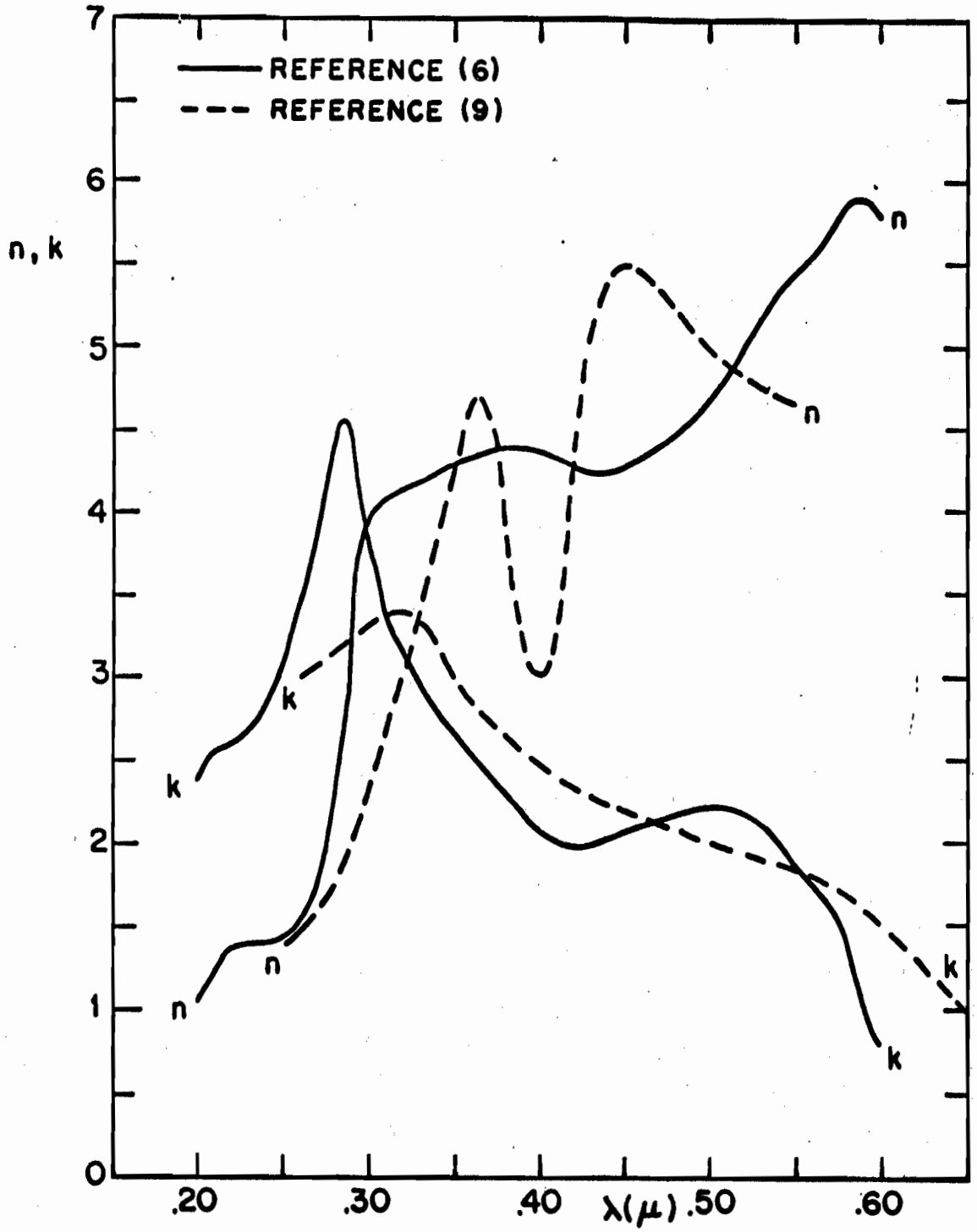

FIG. 1-5c GEBBIE, 1952 (9).

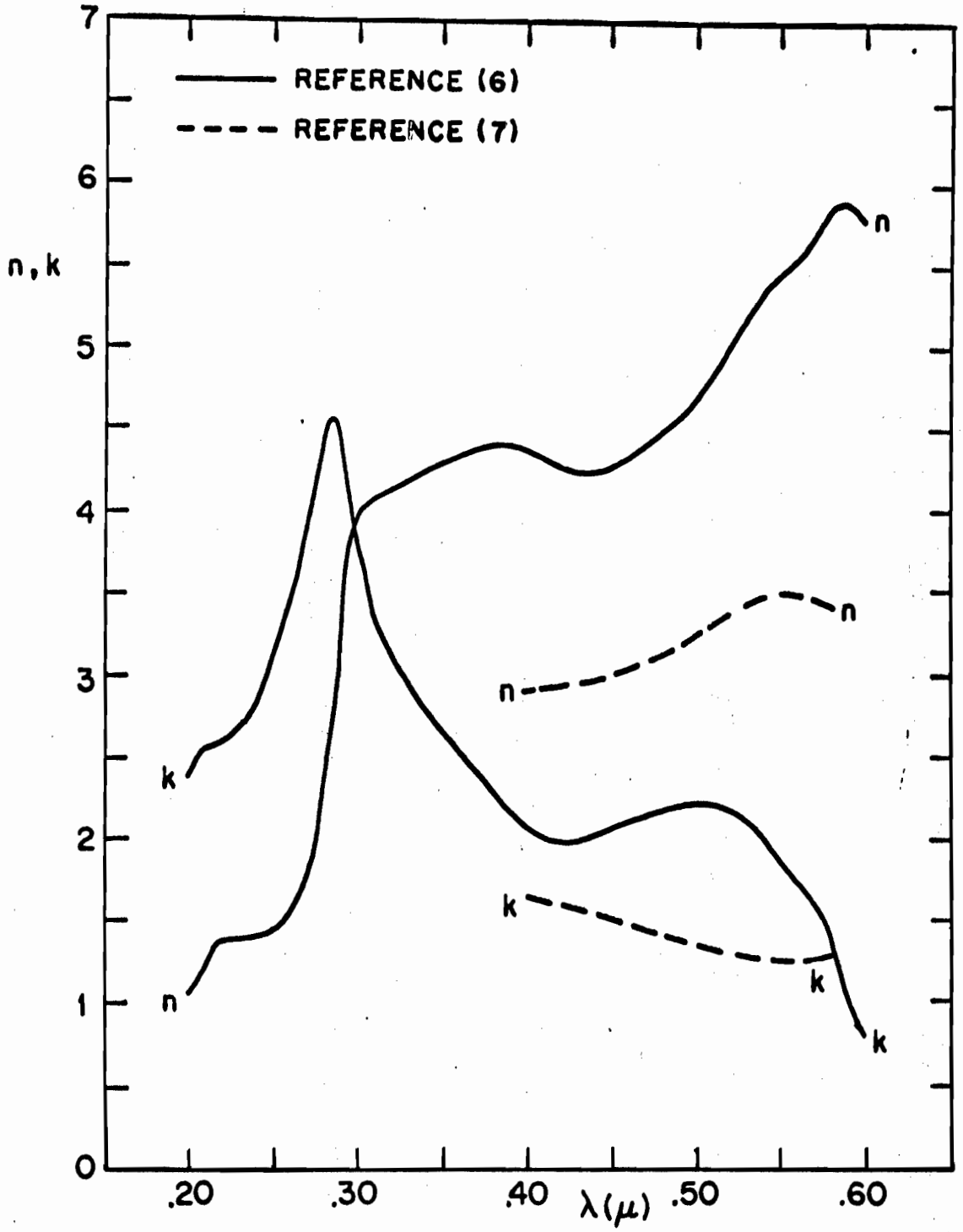

FIG. 1-5a OPTICAL CONSTANTS OBTAINED BY OTHER WORKERS FROM GERMANIUM THIN FILMS.
a. O'BRYAN, 1936 (7).

be discussed in the next two subsections.

3. Results Prior to 1950.

This date roughly marks the beginning of the period when the importance of the crystal structure of the films with regard to their optical properties started to be stressed. The results prior to this date are now discussed.

The first results reported for the optical constants of germanium thin films were by O'Bryan [7] and are displayed in Fig. 1-5a with those of reference 6. They bear little resemblance to each other. O'Bryan's work was quite early (1936) and his films were of undetermined crystalline quality (probably amorphous). He calculated the optical constants from reflectivity measurements at different angles of incidence.

The next data were taken by Brattain and Briggs in 1949 [8]; they are shown in Fig. 1-5b. Again we have depressingly little correspondence with the later Kramers-Kronig results. Their films were deposited on glass, quartz, and CaF_2 slides which were sometimes heated to 150°C during evaporation. After deposition, the films were post-annealed at 400°C but no attempt was made to measure the influence on crystalline perfection (the results of Chapter Four indicate that these films were probably amorphous or nearly so). The optical constants were calculated from the film reflectance and transmittance.

E. REVIEW OF THE ATTEMPTS TO DETERMINE THE OPTICAL CONSTANTS OF GERMANIUM THIN FILMS

1. Skin Depth of Germanium.

In order to gain an appreciation of the sample thicknesses that must be considered when contemplating the transmission of light through germanium, Fig. 1-4 was constructed from the data of reference 6. The skin depth was calculated directly from k with equation (1-25b). We see that at the Σ, X transition at 2800Å, the skin depth is only about 40Å which for germanium is merely eight interatomic distances. Assuming a lower limit for the measurement of transmission of 10^{-3} imposes a maximum sample thickness of about 300Å or 60 atoms. Obviously such samples are impossible to obtain through reduction of the bulk material by conventional grinding and polishing.

2. Preparation of Thin Films.

The main discussion of this topic will be given in Chapter Two. Here we wish briefly to indicate how the problem of preparing thin samples is overcome. The general procedure is to heat a piece of bulk germanium in a vacuum to such a temperature that it begins to vaporize appreciably. A suitable transparent substrate is placed in the vapor stream so as to cause a film of germanium to be deposited on it. The thickness is varied by varying the exposure time. This procedure is that which was used in the work to

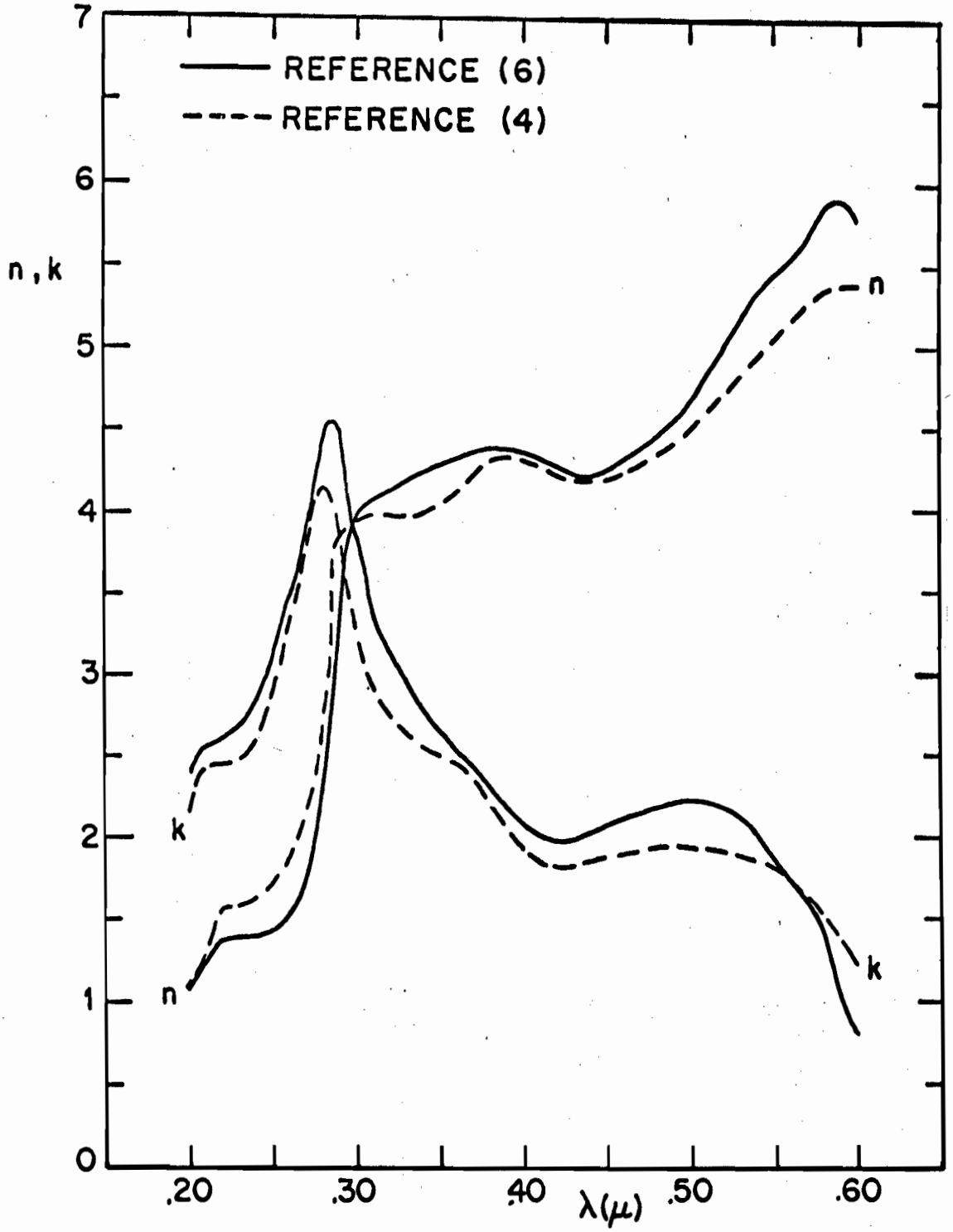

FIG. 1-3b THE KRAMERS-KRONIG RESULTS FOR THE OPTICAL CONSTANTS OF GERMANIUM.

[3], and these constants are also given in Fig. 1-3b along with the previous values. Therefore, by comparing the reflectivities shown in Fig. 1-3a with the optical constants derived therefrom in Fig. 1-3b, we can say that for germanium at least, it appears that variations of 2% to 5% absolute in the reflectivity will cause variations up to one-half of an optical constant in the Kramers-Kronig result.

The dispersion analysis method is presently being widely used to obtain the optical constants of solids. It has the disadvantage that one has to use extrapolation procedures, but it remains to be seen how sensitive the results really are to them. In addition, surface conditions can vary widely. In Fig. 1-3a, Philipp's and Taft's data were taken from a polished and etched sample as was that of Tauc and Abraham; whereas, the data of Donovan, et al., were obtained from an electropolished sample whose surface was of both high optical and crystalline quality. The reflectivity data of Donovan, et al., can be considered authoritative and the optical constants calculated from them by Philipp will be taken as the standard for this work.

3. Photometric Measurements.

By photometric measurements we will mean those methods which measure light intensity ratios such as reflectivity and transmission.

the input may be a current and the output a voltage, the response function thereby being an impedance. The system equations are usually written in terms of their Fourier transforms, namely, $E(\omega) = Z(\omega)\, I(\omega)$, where in general all three quantities are complex functions of the complex variable ω. However, the real and imaginary parts of the impedance are by no means independent of one another [23]. This is because the condition of causality requires that $Z(\omega)$ be analytic in some half-plane of the complex ω plane, thus allowing us to integrate the Cauchy-Riemann equations, which express the real and imaginary parts of $Z(\omega)$ in terms of each other, by means of Cauchy's integral formula. In optics, we can consider equation (1-29a) as being analogous to our Ohm's law above, with ρ being the linear response function. If we express ρ in the form of equation (1-32a), enforce the physical requirement that its inverse Fourier transform be real, and apply the reasoning outlined above, it can be shown that [1]:

$$\psi(\omega) = \frac{\omega}{\pi} \int_0^\infty \frac{\ln \frac{R(\omega')}{R(\omega)}\, d\omega'}{\omega^2 - \omega'^2} \tag{1-39a}$$

$$\ln R(\omega) = \frac{4}{\pi} \int_0^\infty \frac{\omega' \psi(\omega') - \omega\, \psi(\omega)}{\omega'^2 - \omega^2}\, d\omega' \,. \tag{1-39b}$$

Furthermore, equations (1-32b) and (1-32c) can be inverted to give:

this reflectivity peak is very sharp. The small peak near 2100Å has tentatively been assigned to the $L_{3'} \rightarrow L_3$ transition, which is not explicitly shown in Fig. 1-2.

D. REVIEW OF THE METHODS OF DETERMINING THE OPTICAL CONSTANTS OF SOLIDS

1. Polarimetric Measurements.

This method was originally formulated by Drude [20] and has been used by Archer [21] to obtain the optical constants of germanium over a limited wavelength range. It involves the use of a beam of plane polarized monochromatic light in 45° azimuth obliquely incident on a reflecting surface. This beam may be thought of as two in-phase orthogonal plane wave components of equal amplitude; one in the plane of incidence and the other normal to it. After reflection, these components will be out of phase by the angle Δ and the ratio of their amplitudes can be expressed by the quantity $\tan \Psi$. The dependence of these quantities on the optical constants is given by [21]:

$$\frac{1 - e^{i\Delta} \tan \Psi}{1 + e^{i\Delta} \tan \Psi} = \left\{ \frac{n^2 - k^2 \sin^2 \varphi - i\, 2nk}{\tan \varphi \sin \varphi} \right\}^{\frac{1}{2}} \tag{1-38}$$

where φ is the angle of incidence. The reflected components are brought back into phase by a Babinet-Soleil compensator which is essentially a tunable quarter-wave plate. This yields Δ while rotating an analyzer to an extinction position for the now plane

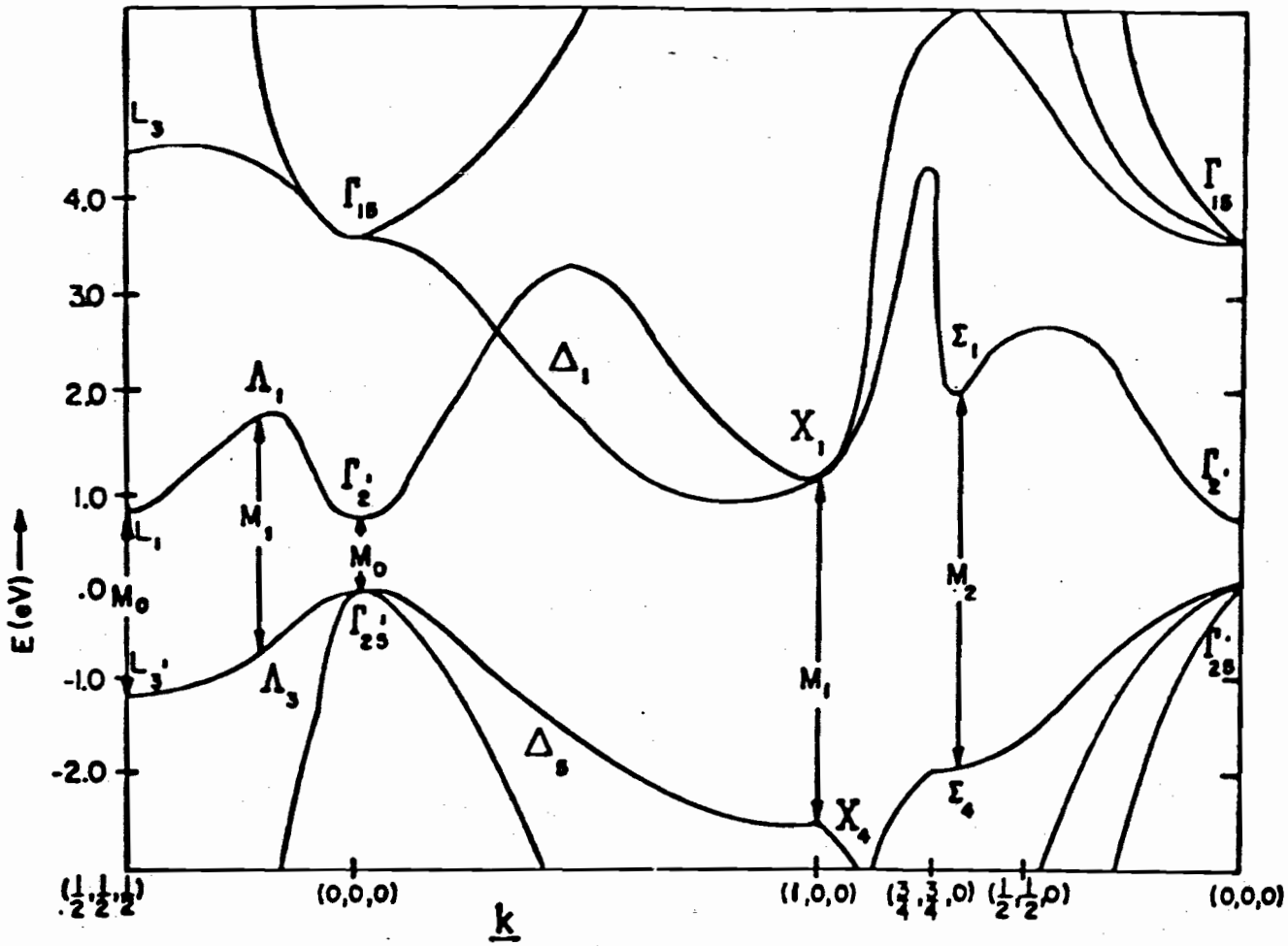

FIG. 1-2 PSEUDOPOTENTIAL ENERGY BANDS OF GERMANIUM AS CALCULATED BY BRUST WITH SOME OF THE PRINCIPAL TRANSITIONS INDICATED.

C. THE BAND STRUCTURE OF GERMANIUM

The band theory of covalent semiconductors has become well established during the past decade. It appears to give an excellent description of their optical properties for energies at least up to 20 eV. Much of our knowledge about the band structure of materials has been gained through experiment; however, we have usually been limited to exploring only those portions of the band that lie near symmetry points of the first Brillouin zone. The advent of the pseudopotential method [14] now allows a fairly accurate theoretical description of the band structure in a region of about 10 ev about the energy gap. These calculations have been a great aid in the interpretation of the visible and ultraviolet optical spectra of semiconductors [15].

The pseudopotential energy bands of germanium have been calculated by Brust [15] and are shown in Fig. 1-2. The notation used to label the bands and symmetry points is that of Bouckaert, Smoluchowski, and Wigner [16]. Also shown in Fig. 1-2 are some of the important interband transitions. In order to demonstrate their connection with the reflectivity spectra of bulk germanium shown in Fig. 1-3a, we will outline how one proceeds from the theoretical band structure to the deduction of the optical constants. Let us consider the following simplifications to equation (1-34):

The one-electron formulation makes contact with the macroscopic theory through the definition of the quantum mechanical current density:

$$\underline{J}' \equiv \left\langle \frac{e}{m} \left(\underline{p} + \frac{e}{c} \underline{A} \right) \right\rangle \tag{1-33}$$

and through the assumption that the $\underline{J}'$ of this equation is identical to that of equation (1-11). Here e is the electronic charge and m its mass, while $\underline{p}$ is the momentum and $\underline{A}$ is the vector potential of the local field. The procedure is then to calculate the expectation value of the canonical momentum $\underline{p} + \frac{e}{c} \underline{A}$ in a suitable representation to terms linear in the electric field and apply equations (1-11) and (1-14) to obtain $\tilde{\epsilon}$ from which the optical constants can be found by equation (1-22). The right-hand side of equation (1-33) has been evaluated by Ehrenreich and Cohen using density matrix methods [12]. Their method included many body effects by describing them as the interaction of a single electron with a self-consistent electromagnetic field. The dielectric constant which results for a Bloch representation and an incident field whose wavelength is much greater than the interatomic spacing is as follows [12]:

$$\tilde{\epsilon}(\omega) = 1 - \frac{(e/\pi)^2}{m} \int d^3k \, \Sigma'_{\ell\ell'} \, f_\ell(\underline{k}) \, f^{\mu}_{\ell'\ell} \times \frac{(\omega^2 - \omega^2_{\ell\ell'}) - \tau^{-2}_{\ell\ell'} - i\, 2\omega\, \tau^{-1}_{\ell\ell'}}{[(\omega - \omega_{\ell\ell'})^2 + \tau^{-2}_{\ell\ell'}][(\omega + \omega_{\ell\ell'})^2 + \tau^{-2}_{\ell\ell'}]} \tag{1-34}$$

In view of equation (1-24), we need only consider the optical response parameters for the electric vector. Defining the complex reflectivity and transmissivity coefficients as

$$\rho \equiv \frac{E_r}{E_i} \tag{1-29a}$$

$$\tau \equiv \frac{E_t}{E_i} \tag{1-29b}$$

respectively, we have immediately from equations (1-27), (1-28), and (1-19):

$$\rho = \frac{\tilde{k}_1 - \tilde{k}_2}{\tilde{k}_1 + \tilde{k}_2} = \frac{\tilde{n}_1 - \tilde{n}_2}{\tilde{n}_1 + \tilde{n}_2} \tag{1-30a}$$

$$\tau = \frac{2\tilde{k}_1}{\tilde{k}_1 + \tilde{k}_2} = \frac{2\tilde{n}_1}{\tilde{n}_1 + \tilde{n}_2} \, . \tag{1-30b}$$

The present work is concerned with the situation where medium 1 is a dielectric with index of refraction n_s and medium 2 is a conductor with complex index of refraction $\tilde{n}$. Also, we will now concentrate on ρ alone as τ and ρ are related by the expression $\tau - \rho = 1$. We then have:

$$\rho = \frac{n_s - n - ik}{n_s + n + ik} \, . \tag{1-31}$$

If medium 2 is a dielectric with greater optical density than medium 1, then we see that ρ is negative. This implies that under this condition the reflected electric vector undergoes a phase change of 180°. It will be convenient for the development

The derivation of the optical response parameters, the reflectivity and transmissivity coefficients, from the boundary conditions (1-4) will now be considered. In view of the fact that all of the optical measurements in this work were taken near normal incidence, only the normal incidence case will be explicitly derived. It provides a very good approximation for angles of incidence up to 10° and even further if the light is unpolarized [2]. Referring to Figure 1-1, it is seen that the appropriate field vectors are as follows:

$$\underset{\sim}{E}_1 = \underset{\sim}{1}_y[E_i\, e^{i\tilde{k}_1 x} + E_r\, e^{-i\tilde{k}_1 x}] \tag{1-26a}$$

$$\underset{\sim}{H}_1 = \underset{\sim}{1}_z[H_i\, e^{i\tilde{k}_1 x} + H_r\, e^{-i\tilde{k}_1 x}] \tag{1-26b}$$

$$\underset{\sim}{E}_2 = \underset{\sim}{1}_y\, E_t\, e^{i\tilde{k}_2 x} \tag{1-26c}$$

$$\underset{\sim}{H}_2 = \underset{\sim}{1}_z\, H_t\, e^{i\tilde{k}_2 x} \tag{1-26d}$$

where the subscripts 1 and 2 denote the medium, and the subscripts i, r, and t the incident, reflected, and transmitted complex amplitudes, respectively. Application of boundary condition (1-4b) yields

$$E_t - E_i - E_r = 0 \quad , \tag{1-27}$$

and application of boundary condition (1-4c) in conjunction with equation (1-16a) gives:

$$\tilde{k}_2 E_t - \tilde{k}_1 E_i + \tilde{k}_1 E_r = 0 \quad . \tag{1-28}$$

Equation (1-18) shows that the wave vector $\tilde{\underline{k}}$ must be complex. By analogy to the case of plane waves in dielectric media we may define the complex index of refraction through the relation:

$$\tilde{\underline{k}} \equiv (n + ik) \frac{\omega}{c} \underline{1}_k = \tilde{n} \frac{\omega}{c} \underline{1}_k \qquad (1\text{-}19)$$

where $\underline{1}_k$ is the unit vector in the direction of propagation of the wave, n is the real part of the complex index of refraction, or simply, the index of refraction, and k is the extinction coefficient. Unfortunately, there now arises a notational difficulty between $\tilde{\underline{k}}$ the wave vector and k the extinction coefficient. However, it should be noted that almost always the context of the discussion should be sufficient to allow one to differentiate between the two. Substitution of (1-19) into (1-18) yields:

$$\tilde{n}^2 = \tilde{\epsilon} \; . \qquad (1\text{-}20)$$

If we write $\tilde{\epsilon} = \epsilon_1 + i\,\epsilon_2$, we obtain:

$$\epsilon_1 = n^2 - k^2 \qquad (1\text{-}21a)$$

$$\epsilon_2 = 2nk \; . \qquad (1\text{-}21b)$$

Relations (1-21) are very useful as it will be seen that optical measurements are better interpreted in terms of n and k while ϵ_1 and ϵ_2 more easily describe the properties of the media in terms of its microscopic structure. The inverse equations for (1-21) are:

dielectric constant linear operator becomes the well-known complex dielectric constant,

$$\tilde{\epsilon} = \epsilon + i \frac{4\pi\sigma}{\omega} . \tag{1-9}$$

The same analysis can be carried out for the conductivity by defining a new current density by the relation,

$$\begin{aligned} \underline{J}' &= \underline{J} + \frac{1}{4\pi} \frac{\partial \underline{D}}{\partial t} \\ &= \sigma \underline{E} + \frac{1}{4\pi} \epsilon \frac{\partial \underline{E}}{\partial t} \end{aligned} \tag{1-10}$$

which leads to the equations:

$$\underline{J}' = \tilde{\sigma} \underline{E} \tag{1-11}$$

$$\tilde{\sigma} = \sigma + \frac{\epsilon}{4\pi} \frac{\partial}{\partial t} \tag{1-12}$$

and for $\underline{E} \sim \exp(-i\omega t)$,

$$\tilde{\sigma} = \sigma - i \frac{\omega\epsilon}{4\pi} . \tag{1-13}$$

The relationship between the dielectric and conductivity operators can then be found from equation (1-1b) to be:

$$\tilde{\sigma} = \frac{\tilde{\epsilon}}{4\pi} \frac{\partial}{\partial t} . \tag{1-14}$$

We will now apply a plane wave solution to Maxwell's equations (1-1) of the form

$$\underline{E} = \underline{E}_o \, e^{i(\tilde{\underline{k}} \cdot \underline{r} - \omega t)} \tag{1-15a}$$

$$\underline{H} = \underline{H}_o \, e^{i(\tilde{\underline{k}} \cdot \underline{r} - \omega t)} . \tag{1-15b}$$

the total current density, and ρ the total charge density. The equation expressing the conservation of charge is

$$\nabla \cdot \underline{J} = - \frac{\partial \rho}{\partial t} \tag{1-2}$$

and the power flow is given by Poynting's vector, viz.,

$$\underline{S} = \frac{c}{4\pi} (\mathrm{Re}\underline{E} \times \mathrm{Re}\underline{H}) \ . \tag{1-3}$$

Expressions giving the relationship between the electromagnetic field vectors on each side of a discontinuity in the material medium will be needed in order to derive the optical response coefficients. The appropriate equations are [1]:

$$\underline{1} \cdot (\underline{B}_2 - \underline{B}_1) = 0 \tag{1-4a}$$

$$\underline{1} \times (\underline{E}_2 - \underline{E}_1) = 0 \tag{1-4b}$$

$$\underline{1} \times (\underline{H}_2 - \underline{H}_1) = \underline{j}_s \tag{1-4c}$$

$$\underline{1} \cdot (\underline{D}_2 - \underline{D}_1) = \rho_s \tag{1-4d}$$

where $\underline{1}$ is the normal unit vector from medium 1 to medium 2, $\underline{j}_s$ is the surface current density, and ρ_s is the surface charge density, both being externally introduced quantities. In this work, we will only consider radiation incident on boundaries containing no such charges or currents.

In order to introduce in an explicit way the manner in which the material medium generates $\underline{D}$ and $\underline{B}$ from $\underline{E}$ and $\underline{H}$, the following relationships are usually defined:

alkali-alkaline earth halides. It is the purpose of this report to demonstrate that the use of epitaxial films, although by no means a panacea, now allows the measurement of the optical properties of materials in the film state which can be extended to and correlated with the optical properties of materials in the bulk state. The problem undertaken for detailed study was the determination of the optical constants of germanium from measurements of the reflection and transmission of thin epitaxial films. The results are compared with those of other experimental methods to calibrate the accuracy of the film optical constants and illustrate the strengths and weaknesses of the film method.

This chapter will be concerned on the one hand with supplying the theoretical foundation for the research and on the other with reviewing attempts which have been made in the past to determine the optical constants of germanium films. The experimental and theoretical work explored the wavelength range 2000 Å to 6000 Å.

Chapter Two describes the techniques of film production, especially those yielding epitaxial films. Analysis of the film crystal structure by reflection electron diffraction (RED) techniques, and examination of the film surface topography by optical microscopy are also discussed.

In Chapter Three the full theoretical development of two photometric methods for the calculation of optical constants of

their consideration as vehicles for further optical research into the high energy, high absorption spectral regions.

(2) The use of epitaxial semiconductor films to calculate optical constants will supplement, but not supplant, other methods such as polarimetry and dispersion analysis.

ABSTRACT

This report describes an investigation into the optical properties of thin germanium films. The central topic is the deduction of the optical constants from photometric measurements on epitaxial films on CaF_2 in the wavelength range 2000 - 6000 Å. Methods of film production are discussed, and the effect of deposition parameters on the crystallinity and reflectivity of films on fused quartz and CaF_2 are reported. The principal conclusion is that epitaxial films give excellent agreement with bulk single crystal material as regards interband transition structure in their reflectivity and transmissivity coefficients R and T. However, the over-all amplitudes of R and T for films are strongly governed by residual surface roughness effects. These cause the magnitude of R, in the region 2000 - 3500 Å, to depart considerably from that of carefully prepared bulk surfaces.

Theoretical studies are carried out on the accuracy of derivation of the optical constants n and k from measurements of normal incidence R and T on a single film. Another model also considered is the recovery of n and k from measurements of the transmissivities of two films of different thicknesses. For each of these methods, the first order dependence of n and k on the photometric quantities was calculated using appropriate theoretical equations and optical constants from dispersion analyses. The

TABLE OF CONTENTS